To the Graduate Council:

I am submitting herewith a dissertation written by Chenghe Xiao entitled "Laser-Induced Reaction Alumina Coating on Ceramic Composite for High Temperature Corrosion Protection." I have examined the final copy of this dissertation for form and content and recommend that it be accepted in partial fulfillment of the requirements for the degree of the Doctor of Philosophy, with a major in Engineering Science and Mechanics.

Mary Helen McCay

Mary Helen McCay, Major Professor

We have read this dissertation
and recommend its acceptance:

J. Wayne McCay

R. Engel

Accepted for the Council:

Associate Vice Chancellor and
Dean for the Graduate School

LASER-INDUCED REACTION ALUMINA COATING ON CERAMIC COMPOSITE

A Dissertation

Presented for the

Doctor of Philosophy

Degree

The University of Tennessee, Knoxville

Chenghe Xiao

May 1997

DEDICATION

To

my family and friends

ACKNOWLEDGMENTS

The author gratefully acknowledge the support to this work by the United States Department of Energy under Grant No. DE-FG22-93PC93225 at the University of Tennessee Space Institute, with Mr. Bill Boss as Project Manager.

The author would like to express his sincere appreciation to his major professor and committee chairman Dr. Mary Helen McCay for her academic advice, guidance and invaluable help throughout the writing of this dissertation. Appreciation is also expressed to the other members of the committee, Dr. Lloyd W. Crawford, Dr. Naren Dahotre, Dr. Remi Engels and Dr. T. Dwayne McCay for their help and advice.

Special thanks to Dr. Dahotre for his help, support, guidance and supervision throughout the development of this research work. The author is also specially grateful to Mr. Bill Boss, supervisor of the author's graduate research assistantship, for his kindly help and support throughout this work and during the author's stay at UTSI.

Many thanks to Mr. Brent Blaha, Mr. Jim Hornkohl, Ms. Kathy Parks, Dr. Vlad Semark, Mr. Mike Sharp, Dr. Feng Sun, Mr. Marvis White, Mr. Jon Winkler, and Mr. Newton Wright for their great assistance in the laboratory, to Ms. Mary Lo and Ms. Brenda Brooks for their help in searching literature, and to Dr. Edwin Gleason and Ms. Callie Taylor for their help during the author's study at UTSI.

Most of all, the author would like to thank his parents, wife and daughter for their constant support, encouragement, and great sacrifices throughout this endeavor.

ABSTRACT

Silicon carbide ceramics are susceptible to corrosion by certain industrial furnace environments. It is also true for a new class of silicon carbide-particulate reinforced alumina-matrix composite ($SiC_{(P)}/Al_2O_3$) since it contains more than 55% of SiC particulate within the composite. This behavior would limit the use of $SiC_{(P)}/Al_2O_3$ composites in ceramic heat exchangers. Because oxide ceramics corrode substantially less in the same environments, a laser-induced reaction alumina coating technique has been developed for improving corrosion resistance of the $SiC_{(P)}/Al_2O_3$ composite. Specimens with and without the laser-induced reaction alumina coating were subjected to corrosion testing at 1200 °C in an air atmosphere containing Na_2CO_3 for 50 ~ 200 hours. Corroded specimens were characterized via x-ray diffraction (XRD), scanning electron microscopy (SEM), and energy dispersive spectrometer (EDS).

The uncoated SiC_P/Al_2O_3 composite samples experienced an initial increase in weight during the exposure to Na_2CO_3 at 1200°C due to the oxidation of residual aluminum metal in the composite. There was no significant weight change difference experienced during exposure times between 50 and 200 hours. The oxidation layer formed on the as-received composite surface consisted of Si and Al_2O_3 (after washing with a HF solution). The oxidation layer grew outward and inward from the original surface of the composite. The growth rate in the outward direction was faster than in the inward direction. The formation of the Si/Al_2O_3 oxidation layer on the as-received composite was nonuniform, and localized corrosion was observed.

The coated samples experienced very little mass increase. The laser-induced reaction alumina coating effectively provided protection for the SiC_P/Al_2O_3 composite by keeping the corrodents from contacting the composite and by the formation of some refractory compounds such as $Na_2OAl_2O_3SiO_2$ and $Na_2Al_{22}O_{34}$. After exposure to 1200°C for 200 hours, the bonding between the laser-induced reaction alumina coating and the composite appeared to be unattacked. For both the coated and uncoated samples, porosity within the composite increased after exposure due to the reaction: $3SiO_2(s) + 4Al(l) \rightarrow 2Al_2O_3(s) + Si(s)$.

TABLE OF CONTENTS

CHAPTER			PAGE
1.	INTRODUCTION		1
2.	BACKGROUND		7
	2.1	High Temperature Corrosion of Ceramics	7
		A. Oxidation	7
		B. Gaseous Corrosion	8
		C. Hot Corrosion	11
		D. Corrosion in Heat Engine	14
		E. High Temperature Heat Exchanger	16
	2.2	Laser Coating Processing	23
3.	EXPERIMENTAL PROCEDURES		26
	3.1	Laser Coating Processing	26
		A. Material and Specimen	26
		B. PVD Precoating	29
		C. Laser Processing	30
		D. Post processing of the samples Treated by Laser Coating Processing	34
	3.2	Mechanical Testing	34
	3.3	Hot Corrosion Experiment	38

4. RESULTS AND DISCUSSIONS....41

4.1 Laser-Induced Reaction Alumina Coating....41

4.2 Mechanical Testing....56

4.3 Corrosion of $SiC_{(P)}/Al_2O_3$ Composite....58

A. Corrosion of as-received $SiC_{(P)}/Al_2O_3$ Composite....60

B. Corrosion $SiC_{(P)}/Al_2O_3$ Composite with Laser-Induce Reaction Alumina Coating....75

5. CONCLUSIONS....85

LIST OF REFERENCES....87

VITA....99

LIST OF TABLES

Table		Page
3-1	Characteristics of $SiC_{(P)}/Al_2O_3$ Composites Substrate	27
3-2	The parameters used for PVD coating of titanium and aluminum	30
3-3	Laser Processing Parameters	33
3-4	Parameters Used for Three-point Bend Testing	37
3-5	As-received Sample Dimensions	37
3-6	Laser-Induced Reaction Alumina Coated Sample Dimensions	38
4-1	Laser Processing Parameters Used During Laser Induced Reaction Coating of Ceramics with Dynamic Fluidized Bed Powder Feeder	42
4-2	Three-Point Bending Test Results for the As-Received Samples	56
4-3	Three-Point Bending Test Results for the Laser Coated Samples	57
4-4	Summary of Three-Point Bend Testing Results	57

LIST OF FIGURES

Figure **Page**

3-1 Scanning electron micro-graphs of the as-received substrate material.....28

3-2 Scanning electron micro-graph of aluminum powder.....29

3-3 Schematic diagram of the experimental set-up for laser coating.....31

3-4 Derivation of 3-point flexure formulas for a rectangular bar.....35

3-5 Sample dimensions.....36

4-1 Overviews of topographical features of a laser-induced alumina coating on $SiC_{(P)}/Al_2O_3$ composite samples.....45

4-2 Magnified views of some samples in the Figure 4-1.....47

4-3 SEM photograph of a high magnification view for the sample from trial #28....48

4-4 Cross-sectional view of the laser-induced reaction-coated $SiC_{(P)}/Al_2O_3$.....49

4-5 X-ray diffraction analysis of laser-induced reaction-coated $SiC_{(P)}/Al_2O_3$.....50

4-6 Free energy of formation as a function of temperature for SiO_2, TiO_2 and $(2/3)Al_2O_3$.....54

4-7 Free energy of formation as a function of temperature for SiC and $(1/3)Al_4C_3$..55

4-8 Weight change of SiC_P/Al_2O_3 composite specimens after exposure at 1200°C to a Na_2O_3 layer (after the corrosion products were removed by a HF solution..59

4-9 Optical microphotograph of cross-sectional view of the SiC_P/Al_2O_3 composite corroded at 1200°C for 150 hours after silicates removed with a HF solution showing Si/Al_2O_3 oxidation product on surface.....61

4-10 X-ray diffraction pattern of the as-received composite.....63

4-11 Al-Si phase diagram[95].....64

4-12 X-ray diffraction patterns of the specimens without the laser-induced reaction alumina coating after the corrosion products were removed with a HF solution.....68

4-13 SEM photograph of a cross-sectional view and elemental x-ray maps of the SiC_P/Al_2O_3 composite corroded at 1200°C for 50 hours (silicates removed with a HF solution).....70

4-14 SEM photograph of a cross-sectional view and elemental x-ray maps of the SiC_P/Al_2O_3 composite corroded at 1200°C for 200 hours (silicates removed with a HF solution).....71

4-15 Optical microphotograph of a cross-sectional views for SiC_P/Al_2O_3 composite corroded at 1200°C after silicates removed with a HF solution.....72

4-16 SEM photograph of surface view of specimen exposed at 1200°C for 50 hours showing glassy layer in center part (before the corrosion products were removed by a HF solution).....74

4-17 SEM photograph of magnified view of the glassy area shown in Figure 4-16 and its elemental x-ray maps.....76

4-18 X-ray diffraction patterns of specimens without laser-induced reaction

alumina coating before corrosion products were removed by a HF solution.....77

4-19 SEM photograph of a surface view of structure underlying glass phase (glassy phase removed with a HF solution) and elemental x-ray maps.....78

4-20 Optical microphotographs of cross-sectional views for the specimens.....80

4-21 SEM photograph of a cross-sectional view and elemental x-ray maps of the SiC_P/Al_2O_3 composite with the laser-induced reaction alumina coating corroded at 1200°C for 50 hours after washing with a HF solution.....81

4-22 X-ray diffraction patterns of specimens with the laser-induced reaction alumina coating before the corrosion products removed by HF solution.....83

4-23 X-ray diffraction patterns of specimens with the laser-induced reaction alumina coating after the corrosion products removed by a HF solution.....84

NOMENCLATURE

B	width of sample coupon (mm)
c	thickness of sample coupon (mm)
g	gas status
ΔG	Gibbs free energy of reaction
l	liquid status
M	moment
P	fracture load (lbs)
s	solid status
σ	flexure stress (Kpsi or Mpa)

CHAPTER 1

INTRODUCTION

With the development of modern industry, ceramic materials applications have been increasingly important and are being considered for high-temperature structural applications, such as heat exchangers, heat turbines, heat engines and magnetohydrodynamic (MHD) generators. Materials used in these systems are exposed to high-temperature corrosive condensed alkali salt environments. Nonoxide silicon-based ceramics, including SiC, Si_3N_4 and $SiC_{(P)}/Al_2O_3$, currently appear to be the leading candidate materials for use in these severe environments due to their high-temperature strength and creep resistance which are superior to those of metals or intermetallics; their thermal conductivity, thermal expansion and thermal shock resistance are also superior to those of refractory oxide ceramics.[1] In particular, SiC particulate-reinforced Al_2O_3-matrix composites have the potential to combine the corrosion resistance of the alumina with the excellent mechanical and thermal properties of silicon carbide. These materials are not thermodynamically stable in air but when placed in highly oxidizing environments obtain adequate oxidation resistance from the formation of a protective SiO_2 film. This film separates the underlying ceramics from the environment.[2] The rate of subsequent oxidation is limited by the slow diffusion transport (up to 1,300°C) through the SiO_2 film.[3]

In spite of these unique properties, it has been reported that SiC, Si_3N_4 and SiC/Al_2O_3 were unstable under condensed hot alkali environments.[4-8] When

contaminates in the environment interfere with the formation of a protective film, these materials may be attacked at a higher rate.[9] Alkali compounds are abundant in incompletely combusted coal gas or complex fused slags. These alkali elements (such as sodium) have been shown to substantially increase the rates of oxidation of silicon carbide and silicon nitride.[10-12] On exposure to incompletely combusted coal environments, a volatile, nonprotective oxide of silicon (SiO) may be formed. The protective silica film also could be dissolved in fused coal ash slags, resulting in a nonprotective liquid film on the surface. Alkali-accelerated corrosion of silicon-based ceramics is usually associated with the formation of liquid silicate or sulfate on the surface of ceramic by "hot corrosion."[13-15] It is possible that the oxidation rate of silicon ceramics will be accelerated due to the continual removal of the protective layer of SiO_2, for example, by erosion, by dissolution in a glassy coating formed by impinging bed materials, or by the formation of SiO vapor rather than SiO_2. A possible remedy to the corrosion problem is a protective coating on the ceramics.

Oxide ceramics have superior corrosion resistance when compared with SiC and Si_3N_4. In several tests where silicon-based ceramics corroded severely, oxide ceramics corroded substantially less.[16-17] Alumina ceramics were particularly resistant to corrosion because the transport of aluminum and oxygen through alumina is extremely slow compared to transport through most other oxides.[18-20] For example, it has been reported that dense alumina ceramics have two to four times greater corrosion resistance than SiC in an advanced glass melting environment.[21] Federe and Jones reported that while SiC corroded at a projected rate of 0.5 mm/year in an aluminum remelt furnace,

alumina was essentially unaffected.[22] Although the oxide ceramics have greater corrosion properties, their lower thermal conductivity and often inferior thermal shock resistance makes them less desirable than the silicon-based ceramics for heat transfer materials.

In an alternative approach, ceramic oxide coatings could be applied to silicon-based heat exchanger tubes combining the superior thermal shock resistance and thermal conductivity of SiC or Si_3N_4 with the improved corrosion resistance of the oxide. For this approach to be successful, however, coatings must be adherent to the SiC substrate and possess adequate resistance to thermal stresses generated during service of the recuperator. Thus, the most effective method to develop oxidation resistance in alloys and coatings at high temperatures above 900°C is to form a continuous layer of α-alumina.[23-24] To be successful, however, the effective use of alumina in the development of these scales and their adherence to various ceramic substrates must be resolved.

Few research efforts related to ceramic coatings on ceramics have been reported in the available open literature, partly due to the inherent problems associated with the process. The conventional methods used are chemical vapor deposition (CVD), physical vapor deposition (PVD), sol-gel, air spraying and plasma spraying, electron beam-physical vapor deposition (EBPVD). None of these processes is fully satisfactory because the coatings produced suffer from excessive porosity, inclusions, microcracks, coating segmentation and poor adhesion. This leads to premature cracking, degradation, and failure by internal sulfidation, spallation, reduced mechanical strain, pitting

corrosion, condensed salt penetration, and oxygen penetration at high temperature.[25-26] Poor adhesion appears to be the major problem because all of these coatings produced by conventional methods are mechanically bonded with the substrate.

Laser-induced cladding, a fairly new technique, provides the possibility of an improved method for the deposition of high-quality coatings, and offers the following advantages:

- the ability to control dilution and produce ultrafine and/or metastable microstructures;
- the ability to deposit a wide range of materials of high and low melting points;
- the minimal distortion and damage of the underlying substrate;
- the possibility of selectively coating inaccessible and localized areas;
- a rapid deposition rate;
- ready automated;
- a metallurgical bonding between the coating and the substrate (the most important aspect).

Direct melting of condensed alumina powder by a laser in a wide range of power densities (10^4 - 10^6 W/cm^2) and interaction times (0.032 - 2.5 s) has resulted in a dense surface layer, but in most instances adhesion of the layer to the metallic substrate has been inferior and in all cases the layer was highly cracked [27] In the current research, aluminum powder was used instead of alumina powder. At the same time,

aluminum will transform to alumina by a laser-induced reaction in the presence of oxygen.

The objective of this dissertation is to explore the feasibility of laser cladding ceramics on ceramics for high temperature corrosion resistance. It presents preliminary observations and evaluations from a study in laser cladding of Al_2O_3 on the commercially available $SiC_{(P)}/Al_2O_3$ substrate by an in-situ reaction technique. Mechanical bending testing and hot corrosion testing (exposure at 1200°C with a thin sodium carbonate film sprayed on) were conducted on the samples before and after laser coating.

This work is funded by a joint university/industry research grant from the US DOE entitled, "High Performance Materials in Coal Conversion/Utilization". This three year grant was awarded to UTSI in October of 1993. The University of Pennsylvania and Lanxide Corporation are both subcontractors under UTSI program management. The stated objective of the grant is to "test, analyze, and improve the heat and coal slag resistance of Lanxide's $SiC_{(P)}/Al_2O_3$ DIMOX^{TM} ceramic composite tubular materials". In addition to the studying the application of the protective coating, the strength of the material before and after exposure to coal slag at elevated temperature was also investigated at UTSI. Researchers at the University of Pennsylvania were charged with developing a theoretical model of the reactions which occur when the composite material and monolithic SiC were exposed to a hot stream of coal combustion products. In addition to supplying the materials needed for the other tasks, Lanxide Corp.

explored new ways to produce the composite materials which may result in reduced cost, improved properties, and better dimensional tolerances.

CHAPTER 2

BACKGROUND

2.1 High Temperature Corrosion of Ceramics

A. Oxidation

Many engineering operations are conducted at high temperature in an air or oxygen environment. While the oxides and stoichiometric silicates are typically stable at such high temperature in an oxygen or mixed oxygen-nitrogen atmosphere, most of the carbides, nitrides, and borides are not. Si_3N_4 and SiC, which are becoming important commercial ceramics, are typical examples.

At elevated temperature, oxygen interacts with any exposed surface of SiC or Si_3N_4. If the oxygen partial pressure is roughly 1 mm Hg or higher, SiO_2 will form a protective layer at the surface. This is referred to as passive oxidation. The chemical reaction to form silica on silicon carbide and silicon nitride are:

- $2SiC\ (s) + 3O_2\ (g) \rightarrow 2SiO_2\ (s) + 2CO\ (g)$ (2-1)

$Si_3N_4\ (s) + 3O_2\ (g) \rightarrow 3SiO_2\ (s) + 2N_2\ (g)$ (2-2)

Formation of SiO_2 will initially be rapid, but will decrease as thickness of the layer increases. Under these conditions, oxidation will be controlled by oxygen diffusion through the SiO_2 layer and will be parabolic. The oxidation rate increases as temperature increases. At low partial pressure (1 mm Hg or below) of oxygen, inadequate oxygen is present to form a protective SiO_2 layer. Instead, SiO (silicon monoxide) gas forms:

$$SiC\ (s) + 3O_2\ (g) \rightarrow SiO\ (g) + CO\ (g) \qquad (2\text{-}3)$$

$$Si_3N_4\ (s) + 3/2O_2\ (g) \rightarrow 3SiO\ (g) + 2\ N_2\ (g) \qquad (2\text{-}4)$$

This is called active oxidation. It is roughly linear and continuous and the component can be completely consumed. Active oxidation conditions are not common but must kept in mind.

The kinetics of passive oxidation were initially determined by weight gain and dimensional change measurement. More important for some applications such as heat engines, however, is the effect of oxidation on the strength of the material. Depending on the ceramic, the temperature, and the initial surface condition, oxidation can increase, decrease, or not affect the strength.[28] For example, a study was performed in which specimens with grinding grooves parallel to the length (longitudinal) and thus parallel to the stressing direction were shown to be much stronger than those with grinding grooves perpendicular to both the length (transverse) and stressing direction. Low-temperature oxidation (1000°C) significantly increased the strength for the transverse machined specimens by blunting or reducing the severity of the surface flaws associated with the grinding damage. High-temperature oxidation completely removed the grinding grooves, but resulted in formation of surface pits, which had an equivalent or worse effect on the strength.

B. Gaseous Corrosion

At high temperatures a material may not be stable in the presence of some gases (i.e. metals in oxygen); the degradation of a material by reaction with gases is called gaseous corrosion. Most high temperature corrosion of ceramics can be attributed to

gaseous corrosion and hot corrosion. Gaseous corrosion of ceramics may occur through a variety of mechanisms just as in the case of the gaseous corrosion of metals and alloys. Moreover, the corrosion processes are ultimately controlled by the nature of the products that are formed as a result of the reaction between the gas and the ceramic.

In metals and alloys, the reaction with the gas is almost always characterized by metallic elements being oxidized via transfer of electron to reducible in the gas. Since the cations of the ceramics are already in the oxidized state and the following corrosion processes can be proposed.

First, the cations may be oxidized to higher states which in the case of oxygen as oxidant would result in oxygen being incorporated into the ceramics. Such a process could result in the formation of new phases or merely a change of stoichiometry of the phase being oxidized. This plays a major role in the degradation of chrome-based refractories subjected to temperature and particularly atmosphere cyclings.

Second, the atoms or molecules of the gas may form more stable compounds with the cations of the ceramics, for example, silicon nitride reacts with oxygen to form silicon dioxide and nitrogen. This type of reaction will depend on the properties of the products formed upon the surface of the ceramic but the effects produced by the elements displaced by the oxygen can also be very important.

A third possibility involves the formation of volatile species such as the reduction of SiO_2 (s) to SiO (g). Such reactions probably would involve diffusion through gaseous boundary layers and could proceed rapidly compared to those of processes involving the formation of condensed phases on the surface of the ceramics.

Finally, molecules in the gas such as SO_3, CO_2 or H_2O may possess a significant affinity for the cationic component or its oxide and react to form compounds such as sulfates, carbonates or hydrates. The rates of such processes will be dependent upon transport through corrosion products and rather complicated mechanisms may prevail. The possible reactions are:

$$SiO_2\,(s) + CO\,(g) \rightarrow SiO\,(g) + CO_2\,(g) \qquad (2\text{-}5)$$

$$SiC\,(s) + CO\,(g) \rightarrow SiO\,(g) + 2C\,(s) \qquad (2\text{-}6)$$

$$2SiC\,(s) + CO_2\,(g) \rightarrow 2SiO\,(g) + 3C\,(s) \qquad (2\text{-}7)$$

$$SiC\,(s) + CO\,(g) + N_2\,(g) + H_2\,(g) \rightarrow SiO\,(g) + 2HCN\,(g) \qquad (2\text{-}8)$$

$$Si_3N_4\,(s) + 3CO\,(g) \rightarrow 3SiO\,(g) + 2N_2\,(g) + 3C\,(s) \qquad (2\text{-}9)$$

$$Si_3N_4\,(s). + 3CO_2\,(g) \rightarrow 3SiO\,(g) + 3CO\,(g) + 2N_2\,(g) \qquad (2\text{-}10)$$

$$Si_3N_4\,(s) + 3H_2S\,(g) \rightarrow 3SiS\,(g) + 3H_2\,(g) + 2\,N_2\,(g) \qquad (2\text{-}11)$$

$$Si_3N_4\,(s) + 3H_2O\,(g) \rightarrow 3SiO\,(g) + 3H_2\,(g) + 2N_2\,(g) \qquad (2\text{-}12)$$

The gaseous corrosion of ceramics is expected to be similar in some respects to the corrosion of ceramics in metals, a subject which has been studied extensively in the literature.[28-30] and which is usually modeled as a dissolution process. The kinetics involves the transport of reactions and products which often determine the overall rate of the corrosion process. The corrosion reaction rate depends on the relative corrosion rate of the various phases, the viscosity of the liquid, the density gradient in the liquid, the concentration gradient in the liquid, the porosity of the solid, the wettability of solid phases by the liquid, the boundary layer at the interface and the geometry of the system. The grain size and the pore structure are major factors in controlling the rate of

dissolution. Fine grain materials dissolve faster than coarse grain materials. The liquid may penetrate into the grain boundaries resulting in engulfment of the solid grains by the liquid.[31, 32] As a result, the influence of the microstructure on the corrosion more complicates the interpretation of corrosion experiments so that for fundamental studies simple systems with simple geometries and microstructures must be used. This is valid also for gaseous corrosion studies since, except for the wetting effect, the grain size, the pore structure and the grain boundaries should play a role similar to liquid corrosion.

There is great deal of literature regarding the oxidation of silicon nitride and silicon carbide,[33,34] however, the only literature on gaseous corrosion of simple oxides appears to be on their reduction and volatilization, particularly for silica. Silica at high temperature under low oxygen pressures volatilizes forming SiO (g) by thermal decomposition and/or by reaction with hydrogen or CO.[35,36] For instance, significant weight losses were observed in wet hydrogen at 1400°C.[37]

Alumina is much more resistant to conditions of this type and tends to lose impurities such as sodium at high temperatures. Significant losses of alumina are only observed at very high temperatures, of the order of 1900°C.[38]

C. Hot Corrosion

In combustion systems, various compounds such as Na_2CO_3, Na_2SO_4 may be generated in addition to combustion gases. Below some temperatures these compounds condense in the engine and often enhance the gaseous corrosion in a complex process named hot corrosion. At their melting points, both Na_2CO_3 and Na_2SO_4 dissociate easily to Na_2O:

$$Na_2CO_3\,(l) \rightarrow Na_2O\,(s) + CO_2\,(g) \qquad (2\text{-}13)$$

$$Na_2SO_4\,(l) \rightarrow Na_2O\,(s) + SO_3\,(g) \qquad (2\text{-}14)$$

These alkali oxides, such as Na_2O, in turn react with silicon-based ceramics to form low melting glass phases with a resultant loss of structural integrity. When normally protective SiO_2 films are contaminated with Na_2O, a lower viscosity and higher oxygen diffusivity result. This allows active oxidation to occur at the SiO_2/SiC interface as the following reaction, causing surface recession of SiC.

$$2SiO_2\,(s) + Na_2O\,(s) \rightarrow Na_2O{\cdot}2(SiO_2)\,(l) \qquad (2\text{-}15)$$

Little hot corrosion has been observed in Na_2SO_4/SO_3 environments for high purity Si_3N_4 and SiC at 1000°C since Na_2SO_4 environment tends to cause impurity effects in ceramics to become a problem at lower temperature than does simple oxidation.[39] However, other studies have revealed that thin films of Na_2CO_3 lead to thick glassy products on SiC at 1000°C. This result is consistent with the removal of the normally protective SiO_2 film to form a non-protective silicate melt.[40, 41] The SiO_2 layer is unstable in the presence of Na_2SO_4 at 1000°C for high oxygen ion activities. Additionally, the penetration of contamination ions (Na, S) down grain boundaries was postulated to lead to altered mechanical properties.[42]

Exposed to a steel soaking pit environment for 800 hr. at ~1250°C, sintered α-SiC forms a silicate-based slag on its surface, but with no measurable loss of α-SiC material; a slight increase in fracture strength following the exposure has been observed.[43] Corrosion of α-SiC by a basic coal slag at 1200°C proceeds by SiO_2 dissolution and formation of low melting silicates, which leades to large corrosion pits.

The pits are responsible for a time-dependent strength degradation of the α-SiC material.[44] Exposure of SiC and Si_3N_4 to a coal-fired gas turbine environment for from 100 to 1000 hours at 1200 to 1425°C results in corrosion/oxidation pits and loss of strength.[45]

McKee and Chatterji[46] have systematically studied the reaction of SiC with various gas and molten salts. They identify three specific cases for molten salts:

For an acidic salt film, such as Na_2SO_4, little or no reaction occurs. This is due to the presence of a stable SiO_2 layer between the salt melt and SiC.

For a basic salt film such as Na_2CO_3, the protective SiO_2 layer is dissolved and accelerated corrosion occurs.

The third case is an oxygen-depleted (carbon-containing) melt. In this case SiO (g) forms at the SiC surface and reacts to form Na_2SiO_4, resulting in rapid corrosion

Blachere and Pettit[39] have studied the corrosion of a variety of ceramics by thin salt films of sulfate under SO_3-SO_2 and oxygen atmospheres at 1000°C. They examined two forms of SiC — chemical vapor deposited (CVD) SiC and hot-pressed SiC. For the Na_2SiO_4/SO_3 films there is relative little reaction, except for SiO_2 globules under the sulfate droplets on the CVD material. For the Na_2SiO_4/O_2 case they report that the hot-pressed SiC exhibits considerable corrosion. The products are rough and contain many bubbles. These observations are consistent with the fact that the protective SiO_2 layer should be dissolved by the more basic melt (i.e., Na_2SiO_4/O_2).

D. Corrosion in Heat Engines

Recently interest has grown in the potential use of ceramics in heat engines as a means of achieving higher operating temperatures and increased efficiency (decreased fuel consumption). SiC and Si_3N_4 currently appear to be leading candidate materials due to their unique combination of high strength and thermal conductivity, low thermal expansion, and good high temperature stability.[47~50]

SiC and Si_3N_4 are being evaluated in gas turbine engines for combustor liners, stator vanes (nonmoving airfoil shapes that guide the hot-gas flow in the optimum direction into the rotor), rotors, and a variety of liners for hot-gas flow through the turbine. Although under operating conditions, these components are exposed to oxidizing atmospheres flowing at moderate to high velocity, oxidation does not appear to be a problem due to the formation of a passive SiO_2 surface layer. However, corrosion can occur as a result of the combined effects of the oxygen plus gaseous, condensed, or particulate impurities introduced via the gas stream. These impurities can either increase the rate of passive oxidation (i.e., modify the transport rate of oxygen through the protective scale), cause active oxidation, or produce compositions which chemically attack the ceramics. The following mechanisms are of particular concern:[51]

1. Change in the chemistry of the SiO_2 layer, increasing the oxygen diffusion rate;
2. Bubble formation, disrupting the protective SiO_2 layer and allowing increased oxygen access;
3. Decreased viscosity of the protective surface layer, which is then swept off the surface by the high velocity gas flow;

4. Formation of a molten composition at the ceramic surface that is a solvent for the ceramics;
5. Localized reducing conditions, decreasing the oxygen partial pressure at the ceramic surface to a level at which active oxidation can occur;
6. Formation of new surface flaws, such as pits or degraded microstructure, which decrease the load-bearing capability of the component.

Singhal[52] has evaluated the dynamic corrosion-erosion behavior of SiC and Si_3N_4 in a pressurized turbine test passage operating at 1100°C, 0.9 MPa pressure, and 152 m/s gas velocity using Exxon No. 2 diesel fuel. After 250 hours of exposure, the surface of the test specimens were smooth and free of adherent surface deposits. Average surface erosion was only 2.3 μm for the SiC and 3 μm for the Si_3N_4 and no strength degradation occurred. Other tests in the same turbine test passage with 4 ppm barium present in the fuel produced drastically different results: massive surface deposits containing barium silicates with iron, magnesium, nickel, chromium, and other trace impurities. This example illustrates that small quantities of some impurities can have a pronounced effect on the corrosion behavior. This is especially important in applications where heavy residual fuels or coal-derived fuels are being considered.

Mckee and Chatterji[53] concluded that SiC at 900°C is inert in H_2, H_2S, and high-purity N_2; that passive oxidation provides protection under normal gas turbine operating conditions or when thin condensed layers of Na_2SO_4 are present in an

oxidizing atmosphere; and that corrosion occurs in the presence of Na_2O, a carbonaceous condensed phase, or a thick Na_2SO_4 surface layer.

Richerson and Yonushonis[54] have evaluated the effect on the strength of Si_3N_4 materials of 50 hr of cyclic oxidation-corrosion at specimen temperature up to 1200°C using a combustor rig burning typical aircraft fuels with 5 ppm sea salt additions. Under conditions where Na_2SO_4 was present in the condensed form, corrosion resulting in slight material recession occurred. This was accompanied by buildup of a glassy surface layer containing many bubbles which appeared to be nucleating at the Si_3N_4 surface. The strength of Si_3N_4 hot pressed with MgO was degraded by 30%. The strength of 2.5-g/cm^3 density reaction-bonded Si_3N_4 was degraded by as much as 45%.

These examples show that both SiC and Si_3N_4 are susceptible to corrosion at high temperatures, especially if impurities are present. However, it should be pointed out that the rates of corrosion are still much lower than for metal gas turbine alloys at much lower temperatures.

E. High Temperature Heat Exchanger

The most efficient of the various types coal gasifiers under development is the slagging design, which operates at relatively high temperatures for more complete conversion of the powdered coal feedstock. The operating temperature is above the melting point of the coal slag, which is tapped from the bottom of the gasifier. As a result of operating at such high temperatures, however, as much as 20% of the energy in

the coal is converted to sensible heat rather than synthetic gas. In order to recover this energy, large heat exchanger systems may be utilized.

With current and projected energy conservation requirements, the use of heat exchangers to recover waste heat is growing in importance. Heat recovered from the exhaust of a furnace is used to preheat the inlet combustion air, so that additional fuel is not required for this purpose. The higher the operating temperature, the greater the benefit. In many cases, however, such as coal gasification, metal and glass melting furnaces, incinerators, and coal-burning furnaces, the discharge gases are either too high in temperature or too corrosive for metal heat exchangers. Thus two important design requirements of the material are high-temperature capability and corrosion resistance. Another is thermal shock resistance since industrial heat exchangers are massive and involve substantial thermal stresses.

High thermal conductivity to maximize the rate of heat transfer and optimize the efficiency of the unit is an additional desirable property of a heat exchanger material, but it is usually of less importance than thermal shock resistance, temperature capability, and corrosion resistance. The major material being used and evaluated for industrial heat exchangers is SiC, primarily in tubular form. Other materials with potential for various types of heat exchangers include Si_3N_4 and mullite.

The raw-gas outlet temperature can exceed 1300°C in slagging gasifiers. The major components of the gas are carbon monoxide and hydrogen, such that relatively reducing conditions exist. The low oxygen partial pressure is accompanied by a moderate sulfur partial pressure, which is defined by the coal feedstock. The prevailing

conditions at the heat exchanger inlet are known to cause structural material wastage via corrosion, sulfidation, and oxidation, as well as degradation of mechanical properties and heat transfer effectiveness as surface scales build up and/or spall off. Even the most durable of the refractory materials cannot withstand extended periods of exposure at temperatures greater than approximately 700°C. This is especially true in the highly reducing coal gasification environments, where hydrogen embrittlement and alkali attack are major problems.[55,56]

Easler[57] has studied the corrosion behavior of silicon carbide materials in a simulated coal gasification environment. Specimens exposed at 1250 and 1300°C for 200 hours with acidic or basic coal-slag coatings exhibited weight loss and corrosion pits. A greater weight loss and the more severe corrosion pits were observed in specimens coated with the basic slag which resulted in decreased strength. A decrease of about 15% was observed when samples were exposed without slag or with an acidic slag coating. A 34% reduction in strength was observed for samples coated with the basic slag.

Another application of heat exchangers is found in the energy intensive glass industry which uses approximately 250 trillion BTU per year, of which 84% is supplied by natural gas.[58] Their gas-fired, regenerative open-hearth furnaces are only 37-45% energy efficient and produce high levels of sulfur oxides, nitrogen oxides and particulate emissions. Because of rising fuel costs and increasingly stringent legislation limiting pollution emissions, the glass industry has sought out innovative systems for melting and forming glass, such as the Advanced Glass Melter (AGM).

A vital part of the AGM design involves recuperative heat exchangers, which produce preheated air for the burner from the hot exhaust gases. Since the flue gases in the AGM have the potential to be very hot (in excess of 1000°C) and may contain high concentrations of corrosive alkali compounds, the use of advanced ceramic materials is necessary to meet these design criteria.

In a series of preliminary tests in a simulated AGM flue environment,[59,60] a new class of silicon carbide-particulate reinforced alumina-matrix (SiC/Al_2O_3) composites[61-63] indicated promise as a material for the heat exchangers. In these tests, sintered α-SiC had adequate thermal and mechanical properties, but was severely attacked by the molten sodium silicate deposited from the combustion gases. High density alumina had adequate corrosion resistance but was too susceptible to thermal shock failure to be seriously considered. The SiC/Al_2O_3 composites have the potentials to combine the corrosion resistance of the alumina with the strength and thermal conductivity of the silicon carbide.

A more detailed investigation was conducted by Keret on the durability of the SiC/Al_2O_3 composite in a simulated glass melting flue environment [64] The dynamic corrosion tests, which were performed at 1000-1300°C for 10-300 hours, consisted of. continuously delivering sodium silicate in the form of micro-sized droplets onto specimens at a 45 degree angle with respect to the horizontal. Results indicated that the composite gained weight through the formation of Al_2O_3/metal oxidation products at all exposure conditions, and that the corrosion removal of material became significant only during the exposure at 1300°C. The dynamic corrosion exposure also caused a

significant loss in the strength of the composite at room temperature. The strengths of the SiC/Al_2O_3 composite for the as-received condition and after the exposures to dynamic corrosion for 300 hours at 1000°C and 100 hours at 1300°C are 480, 98, and 130 MPa respectively.

Magnetohydrodynamic (MHD) generators represent still higher temperature and more severe corrosion requirements for ceramic materials. Operation temperatures are in the range 1600 to 2500°C. The MHD generator produces electricity by rapidly. passing a moving conductive gas through a magnetic field. Conductivity in the gas is achieved at high temperature by seeding the gas with a salt such as K_2SO_4 or K_2CO_3 which has a low ionization potential. This can result in an electron density of 10^{12} to 10^{13} free electrons per cubic centimeter (compared to 10^{22} to 10^{23} for a metal conductor). In an open-cycle MHD generator, the moving high temperature gas can be supplied by coal or other fossil fuel combustion. In order to economically achieve the desired efficiency in the MHD, a high temperature high pressure air heater will be needed. Such a heat exchanger must work in such a severe environment that no current metallic superalloy can be used and only ceramic materials can be considered. A variety of ceramic and ceramic matrix composite materials have been investigated for use in the high temperature air heater. Among those which have been tested in the MHD facility at UTSI (from approximately 1100 to 1600°C) are silicon carbide, magnesia aluminum spinel, zirconia, chrome magnesia, boron nitride, alumina and SiC/Al_2O_3 composite. Of all of the materials tested, only one material yielded hopeful results, the $SiC_{(P)}/Al_2O_3$ ceramic matrix composite fabricated by Lanxide. This material demonstrated a strong

resistance to high temperature corrosion along with excellent resistance to thermal shock. No significant loss of material was found to occur after several hundred hours at exposure temperatures up to 1400°C. However, above 1450°C, rapid material removal was experienced in a much shorter period of time than that below 1400°C.[65]

In 1992, a study was conducted by Jon Winkler[66] at UTSI involving mechanical testing of circular rings cut from a $SiC_{(P)}/Al_2O_3$ tube exposed during one of the MHD tests. This study compared the properties of the material, as it was received from the manufacturer, with samples which had been exposed to slag at a tube temperature of approximately 1230°C for 107 hours. The tests showed a slight decrease in characteristic strength after exposure and microscopic examination revealed an increase in porosity associated with exposure temperatures. The porosity in the specimens increased from the as-received samples approximately 2 volume % to 23 volume % for the exposed samples.

A more detailed study was conducted by Peter LaRue[67] at UTSI in 1995. Tubular samples of $SiC_{(P)}/Al_2O_3$ ceramic composite were exposed to a simulated coal combustion environment, with Illinois #6 coal slag, at temperatures of 1100°C, 1260°C, and 1400°C for a period of 200 hours. Additional samples were held at these same temperatures without the application of slag. Subsequent strength testing found that the strength of material decreased as the temperature of exposure was increased, with additional decreases caused by exposure to the coal slag. Furthermore, at 1400°C, a noticeable amount of the tube material was lost. Microscopic examination also indicated that the porosity increased significantly as exposure temperature was

increased. It was postulated that active oxidation of silicon carbide could occur inside the tube and result in the pore formation when the tube was exposed in the reducing environment of MHD exhaust gas. Since the SiC particulate were preferentially attacked compared to the alumina matrix, the corrosion rate of the composite was probably partially limited by the rate of dissolution of the alumina matrix into the coal slag. If the tube surface was continuously covered by an alumina coating, the corrosion rate of the tube should totally be limited by the alumina because alumina possesses a much higher corrosion resistance than that of silicon carbide

In a related program at Oak Ridge National Laboratory (ORNL) on the development of ceramic materials for use in heat recovery equipment for high temperature process furnaces, Federer[68] found that silicon-based ceramics are corroded by alkali compounds contained in combustion gases. Specifically, he found that silicon carbide and silicon nitride ceramics are severely corroded by alkali vapor compounds and the corrosion rates of oxide ceramics increase with increasing silicon dioxide content. Federer attributed this alkali-induced corrosion to the formation of alkali silicates which result from the reaction of alkali oxides, such as Na_2O and K_2O, with the normally protective SiO_2 ceramic film. These alkali silicates, which are molten at temperatures as low as 798 °C (e.g. $Na_2O{\cdot}2SO_2$), cause softening of the SiO_2 film. The resulting enhanced diffusion of oxygen through the altered film causes oxidation of the silicon-based ceramic. Similarly, for composite ceramics which combine silicon and oxide components, the alkali oxides react with the silicon component to form lower melting point silicates, which dissolve the more refractory oxide components, such as

Al_2O_3 and ZrO_2. Therefore, Federer suggests that the oxide-based ceramics, such as alumina and zirconia with limited amounts of SiO_2, are the best candidate ceramic materials for heat exchangers for use with combustion gases which contain alkali vapors.

2.2 Laser Coating Processing

The use of high power energy lasers for surface cladding has been acknowledged as a possible method of surface modification for the last twenty years. A 1976 patent[69] entitled "cladding" involves the use of direct wire feeding under a scanning laser beam. British researchers, however, claim the "shadowing" effect of solid wire does not seem to couple the laser energy as effectively as powder and, hence, powder would be the preferred consumable for surfacing. Powell, for example, has published work using Ni-Cr-Si-B powder fed continuously under a laser beam with a manual powder torch modified to use an argon carrier gas rather than oxy-fuel combustion.[70] Other variations have been devised for direct powder feed into a laser beam (known as direct cladding or cladding).[71~76] Another possibility involves preplacement of powders onto a substrate prior to laser fusing instead of attempting to solve problems of "feeding" a powder consumable directly under or in front of an advancing laser beam. Thermal spray methods, such as oxyacetylene flame spray[77] and plasma spray[78~80] have been used to preplace powder onto a substrate for subsequent laser fusing (known as laser sealing).

The direct cladding by laser was accomplished by melting a limited layer of the underlying substrate and blowing a stream of fine particles of the cladding material which may or may not melt during laser scanning. The laser-induced direct cladding process

produces a metallurgically bonded coating on the substrate. On the other hand, the plasma sprayed layer is primarily mechanically bonded to the substrate and even after the laser sealing process, this layer still maintains mechanical bonding with the substrate. Hence, the laser-induced direct cladding layer has much stronger bonding with the substrate than that of laser sealing. This characteristic is very helpful in obtaining higher corrosion resistance and erosion resistance because of its higher adherence.

Many studies have been conducted on laser interactions with metals and semiconductors, but little has been done in the processing of conventional ceramics with lasers. The laser has been used in the growth of crystals and in the formation of ceramic powders, but attempts to heat ceramic bodies with a high density laser beam have usually resulted in crack formation and degradation.[81] Because of this problem, in comparison to studies on metals, a great deal more care will be required in the building up of ceramic layers or changing surface characteristics of ceramic bodies using a laser. Certain observations of laser interactions with materials suggest possible uses of the laser in ceramic processing. For example, it has been demonstrated that laser power can be used to modify the plasma-sprayed ceramic thermal barrier coatings.[82] During that study, when a less intense beam and/or larger beam and a faster sample speed were used, the surface of the coatings could be densified.

Laser-induced cladding has been used successfully to modify surface properties of materials, particularly for improving wear and corrosion resistance (including high temperature). Up to the present time laser-induced cladding has been mainly used on metal surfaces. It appears that no work has been reported on the laser cladding on a

ceramic substrate surface. In this study, aluminum powder will be used to replace high melting point alumina powder as a coating material so that it is possible to use a less intense beam to lessen or avoid causing cracking of the ceramic substrates during processing.

CHAPTER 3

EXPERIMENT PROCEDURES

3.1 Laser Coating Processing

A. Material and Specimen

Substrate material and specimens Lanxide Corporation's $SiC_{(P)}/Al_2O_3$ DIMOX^{TM} Ceramic Matrix Composite was used as the substrate material. The material was obtained in tubular form with a 50 mm outside diameter and a wall thickness of 5 mm. Lanxide's material designation for this materials was 93-X-3015. It has a density of 3.4 g/cm^3. The composite contains about 45% (by volume) of SiC particulates (which have diameters from 3 to 20 microns), 52% Al_2O_3, 1.6% residual aluminum alloy (left over from the fabrication process), and 1.4% porosity. Characteristics of the $SiC_{(P)}/Al_2O_3$ substrate are summarized in Table 3-1. Figure 3-1 gives surface and cross section views of the substrate material. Specimens of approximate rectangular prism shape, 5 mm thick, 10 mm wide and 30 mm long, were cut from the tube with a diamond saw. All specimens were ultrasonically cleaned in an acetone bath and then thoroughly dried in air.

Table 3-1. Characteristics of $SiC_{(P)}/Al_2O_3$ Composites Substrate

Material Characteristics	
SiC content, volume %	45
Al_2O_3 content, volume %	52
Residual aluminum alloy content, volume %	1.6
Porosity content, volume %	1.4
Density, g/cm^3	3.4
Tube Dimensions, mm	
Outside diameter	50
Inside diameter	40
Wall thickness	5
Specimen Dimension, mm	
Length	30
Width	10
Thickness	5

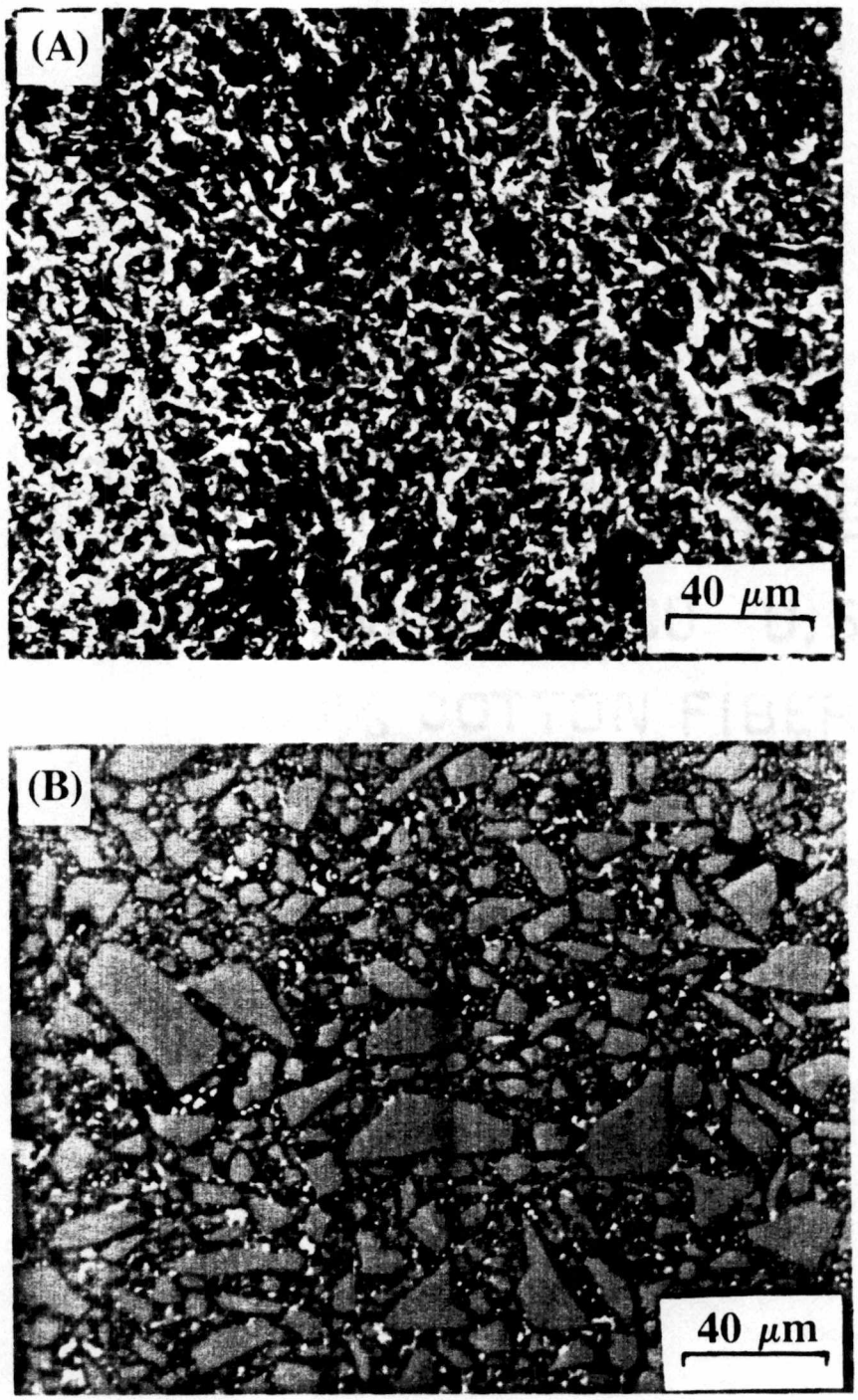

Figure 3-1. Scanning electron micro-graphs of the as-received substrate material: (a) surface view and (b) cross-sectional view.

Aluminum Powder A commercially available atomized aluminum powder from the ALCOA Company was used as the precursor material for coating. The particle size was from 1 μm to 5 μm, and the average size was 2.5 μm. Figure 3-2 shows the particle features. The powder was dried by heating at 120°C in a electric resistance furnace for 5 hours and then cooled at room temperature prior to coating experience.

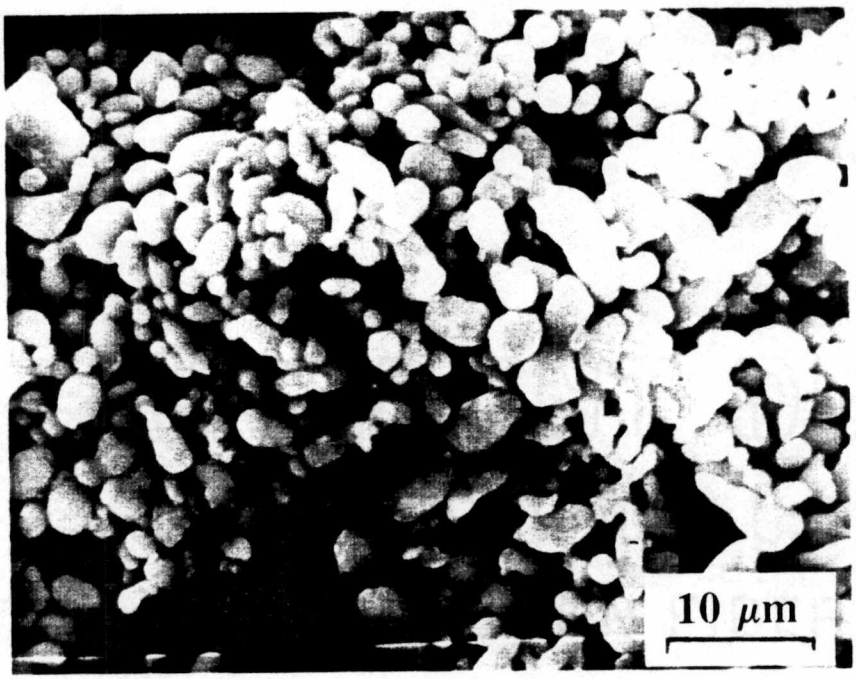

Figure 3-2. Scanning electron micro-graph of aluminum powder.

B. PVD Precoating

In order to create a sound bond and higher wettability between the substrate and the coating material, a bond coat was first deposited on the ceramic substrate prior to the

laser coating process. A bond layer about 5 μm thick of either titanium or aluminum was deposited on the $SiC_{(P)}/Al_2O_3$ substrate using physical vapor deposition (PVD) technique prior to the laser coating process. PVD was applied with a commercially available Dayton Vacuum unit. Multiple samples were produced simultaneously. The sample stage was inclined at 45° and was continuously rotated at 30 rpm around the vertical axis. This arrangement provided the condition for deposition of a uniformly thick bond coat on the substrate surface. The parameters employed for PVD are given in Table 3-2.

Table 3-2. The parameters used for PVD coating of titanium and aluminum

Coating Material	Current (amp)	Voltage (volt)	Vacuum (torr)	Time (min)
Titanium	25-30	80-95	2×10^{-5}	5
Aluminum	15-20	25-40	2×10^{-5}	5

C. Laser Processing

The experimental arrangement for laser coating is shown diagrammatically in Figure 3-3. The experimental set up consists of two units: the laser and the powder feeder system. The laser system, a Rofin-Sinar RS3000 CO_2 laser, was employed for this experiment. The RS3000 laser is a fast axial-flow, radio-frequency (27.12 MHz) excited CO_2 laser with an operating power range from 200 to 3700 Watts. It may be configured to produce TEM_{00}, TEM_{10}, TEM_{20}, or TEM_{01*} spatial modes in a beam which is circularly polarized with external optics. An optical beam delivery system with

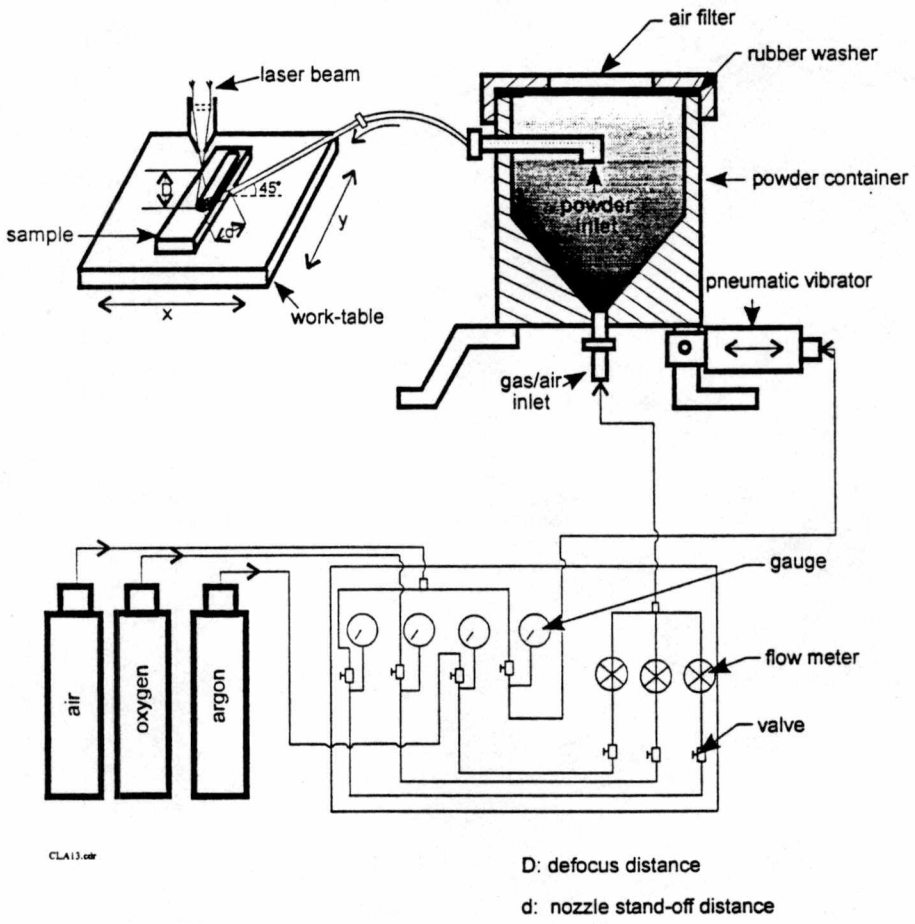

Figure 3-3. Schematic diagram of the experimental set-up for laser coating

a 150 mm focal length gold-plated copper off-axis parabolic mirro provides focusing of the beam to a 300 μm diameter spot size. The laser may be operated in one of four modes: full CW, 5 kHz modulated power, pulse (25 kHz Max.), and superpulse (25 kMz, Max.). A computer numeric controlled (CNC) five-axis Aerotech workstation was used to translate the work-table during laser processing while also providing control of the laser and associated equipments such as flow valves for the cover gas. For the experiments carried out in this study, the laser was operated in 5 kHz modulated power, a quasi-continuous wave (Q-CW) mode. Argon was blown through the nozzle to shroud the work area and also to protect the lens.

As depicted in Figure 3-3, a dynamic fluidized-bed powder feeder (designed and fabricated in the laboratory) delivered the precursor aluminum powder at the laser-substrate interaction region. A pneumatic vibrator in conjunction with high-pressure air/gas separates the powder clusters into individual particles by breaking the weak electrostatic forces between them. The high-pressure air/gas also fluidizes the powder particles and entrains them to the laser-material interaction region via a delivery tube. An air filter at the top of the powder container avoids excessive pressure build-up while ensuring a continuous and smooth powder flow. The air/gas flow rate controls the powder delivery rate. A efficient powder delivery can be achieved by selecting a proper combination of the inlet air/gas flow rate together with the frequency of the pneumatic vibrator. In addition, the inlet gas being a carrier for the powder, it can provide a reactive environment at the laser-material interaction region for conversion of aluminum into an Al_2O_3 ceramic.

Laser in-situ reaction coating of Al_2O_3 with an aluminum powder was initially conducted on an as-received, and a bond-coated (titanium or aluminum) $SiC_{(P)}/Al_2O_3$ substrates. The best pre-existing surface condition was then chosen according to the coating quality. The laser beam, defocused on the sample surface, was scanned continuously with some overlap between consecutive passes to cover the entire surface. The laser processing was carried out with a slight overpressure of oxygen. The main parameters in this coating process are beam power, beam diameter, traverse (or scanning) speed, powder flow rate, and overlap rate. These parameters were varied to identify the optimum conditions for obtaining complete coverage, and a smooth and adherent coating. Large areas of the substrate were covered by making a series of parallel overlapping tracks. The laser processing parameters used are tabulated in Table 3-3.

Table 3-3. Laser Processing Parameters

Laser Power (watts)	150 ~ 1500
Beam Mode	TEM_{10}
Traverse Speed (mm/s)	20 ~ 30
Focal Position (mm)	5 ~ 25 above substrate surface
Shielding Gas (l/min)	Argon (coaxial), 2
Reaction Assist Gas (l/min)	Oxygen, 2
Overlap (%)	30~60
Powder Feeder (mg/s)	50 ~ 250
Powder Outlet Nozzle Angle	30 ~ 60° to the horizontal

D. Post Processing of the Samples Treated by Laser Coating Processing

The initial laser-coated samples were cross-sectioned and mounted in epoxy. Each sample was metallographically prepared by polishing with a series of grit papers for microstructural evaluation. The final polishing was done with a 1 μm diamond paste.

Microstructures and surface topography were studied by optical and scanning electron microscopy (SEM). Chemical composition and phases were determined by energy dispersive spectroscopy (EDS) and x-ray diffractometery (XRD). Throughout these analytical techniques, the optimum conditions (parameters) of laser processing were determined for obtaining a high conversion rate of reaction, complete coverage, and a smooth and adherent coating. All the rest of the samples were laser processed with these optimum parameters and then mechanically and corrosion tested.

3.2 Mechanical Testing

The strength of ceramic materials is generally characterized by bend testing (also referred to as flexure testing). The test specimen can have a circular, square, or rectangular cross section and is uniform along the complete length. Such a specimen is much less expensive to fabricate than a tensile specimen.

Bend testing is conducted with the same kind of universal test machine used for tensile and compressive strength measurements. The test specimen is supported at the ends and the load is applied either at the center (3-point loading) or at two positions (4-point loading). The bend strength is defined as the maximum tensile stress at failure

and is often referred to as the modulus of rupture, or MOR. The bend strength for a rectangular test specimen can be calculated using the general flexure stress formula:

$$\sigma = \frac{Mc}{I}$$

where M is the moment, c the distance from the neutral axis to the tensile surface, and I the moment of inertia. For a rectangular test specimen $I = \frac{b d^3}{12}$ and $c = \frac{d}{2}$, where d is the thickness of the specimen and b is the width. Figure 3-4 illustrates the derivation of 3-point flexure formulas for rectangular bars.

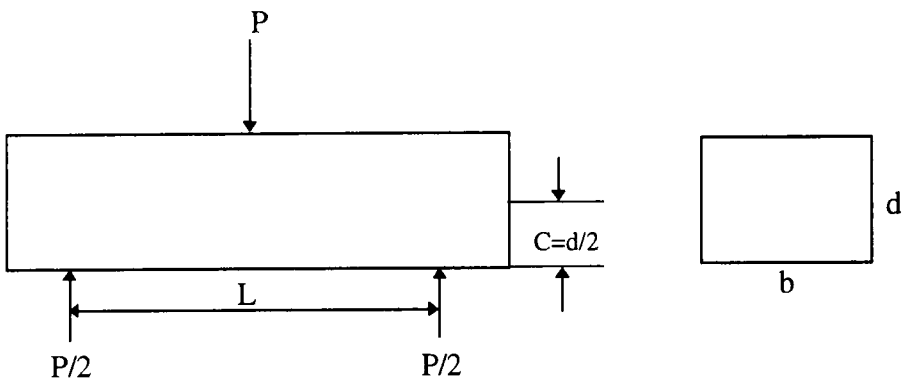

$$M = \frac{L}{2}\frac{P}{2} \qquad I = \frac{bd^3}{12} \qquad \sigma_{3-PT} = MOR = \frac{Mc}{I} = \frac{3PL}{2bd^2}$$

Figure 3-4. Derivation of 3-point flexure formulas for a rectangular bar

The mechanical testing performed in this study was not designed to produce an absolute measured value but rather to detect any difference in the mechanical properties between the as-received material and the laser-treated material (laser induced reaction coated) due to high thermal shock to the material during laser processing. Due to the limitation of small dimensions of testing material available, the three-point bend was used.

Two sets of samples for strength testing were produced from each as-received and laser-induced reaction coated samples. Each set included coupons of approximately 30 mm long and 10 mm wide on the outside surface (the inside surface width was not as the outside surface to be). Figure 3-5 gives sample coupon dimensions. The coupon was roughly considered as rectangular and B ($B = (a+b)/2$) as its width. The bend strength is given by:

$$\sigma = \frac{3PL}{2Bc^2}$$

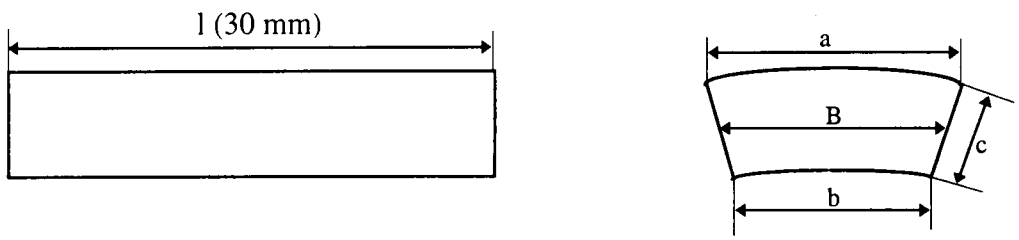

Figure 3-5. Sample dimensions

Ten of these coupons from each of the as-received and laser-induced reaction coated samples were selected for bend testing using an Instron testing machine. Table 3-4 gives the test parameters used in the three point bend tests. Table 3-5 and Table 3-6 give the sample dimensions.

Table 3-4. Parameters Used for Three-point Bend Testing

Load Speed	Normal Load	Record Chart Speed
0.5 mm/min	250 kg.	130 mm/min

Table 3-5. As-received Sample Dimensions (L=22.66 mm)

Sample #	a (mm)	b (mm)	c (mm)	B (mm)
1	9.94	8.26	4.96	9.10
2	9.88	7.52	5.08	8.70
3	9.72	8.84	5.30	9.28
4	9.52	7.68	4.62	8.60
5	10.54	8.72	4.96	9.63
6	9.26	7.62	4.76	8.44
7	9.34	7.90	5.40	8.62
8	12.30	9.58	5.04	10.94
9	9.22	7.26	5.04	8.24
10	10.80	8.26	5.42	9.53
Average	10.05	8.16	5.06	9.11

Table 3-6. Laser-Induced Reaction Alumina Coated Sample Dimensions (L=22.66 mm)

Sample #	a (mm)	b (mm)	c (mm)	B (mm)
1	9.70	8.42	4.80	9.06
2	10.34	8.48	5.04	9.41
3	9.70	8.16	4.82	8.93
4	10.30	8.24	5.40	9.27
5	10.58	8.64	5.44	9.61
6	9.80	8.46	5.24	9.13
7	10.52	8.44	4.94	9.48
8	10.50	9.26	4.96	9.88
9	9.80	8.76	5.14	9.28
10	10.70	9.26	4.80	9.98
Average	10.19	8.61	5.06	9.40

3.3 Hot Corrosion Experiment

The experimental techniques used in hot corrosion studies of ceramics are similar to those in hot corrosion studies of metals. There are two common approaches: (1) Burner studies with a salt solution aspirated in the burner and (2) Laboratory furnace studies with thin salt films.

A burner system comes closer to duplicating actual environments than a laboratory furnace, but burner experiments are expensive and it is difficult to precisely control all operating parameters.

The laboratory furnace corrosion study was employed in this investigation. In a laboratory corrosion study, a thin salt film is sprayed on a ceramic coupon. Then the coupon is placed in a laboratory controlled-atmosphere furnace. Such experiments are inexpensive and allow precise control of temperature, pressure, and salt chemistry. The kinetics of reaction can be followed by continuous weight change measurements or by pulling samples for chemical analysis after various time intervals. The major drawback to these experiments is that they involve a one-time deposition of salt and not a continuous deposition as would occur in an actual condition.

Eight coupons for hot corrosion testing were prepared from both as-received samples and laser-induced reaction coated samples. The sample dimensions were approximately 5 by 10 by 30 mm. All the specimens were sprayed with 2-3 mg/mm^2 coatings of Na_2CO_3 (basic salt) from a saturated aqueous salt solution because a basic salt caused higher corrosion rate than acid salt. The specimens were then exposed to 1200 °C in air for 50, 100, 150 and 200 hours respectively. The exposure temperature was achieved and maintained inside a Pereco^{TM} electric resistance furnace. The furnace was brought up to the 1200°C at a rate of approximately 100°C per hour. Once that temperature was reached, it was held constant (1200 ± 10°C) for the designated period. The hot corrosion testing performed in this study was designed to determine if there was any difference in the corrosion resistance in a basic environment between the as-received material and the laser-induced reaction coated material.

Post-exposure evaluation of the specimens included measurement of weight change, x-ray diffraction (XRD), and scanning electron microscopy (SEM) equipped

with energy dispersive spectrum (EDS) analysis. Initially, the corrosion product layer surface was examined. Next, the corrosion product layer surface was removed with a 10% volume HF in H_2O solution for six hours at 90°C, then the etched substrate was examined. Control samples of the uncorroded as-received $SiC_{(P)}/Al_2O_3$ composite were also subjected to this HF dissolution treatment for comparison purpose. Very little dissolution for the uncorroded samples was observed from weighing the sample before and after the HF dissolution treatment on an analytical balance with a sensitivity of 0.01 mg.

CHAPTER 4

RESULTS AND DISCUSSIONS

4.1 Laser-Induced Reaction Alumina Coating

Some of the laser-induced reaction ceramic coating runs were initially conducted on samples with different pre-existing surface conditions, such as the as-received, Al, and Ti PVD surface coating using some of the laser processing parameters given in the Table 3-3 at different powder feeder nozzle angles (30~60°). These experiments showed that the samples with Ti PVD pre-coating appeared to have the highest wettability for the laser-induced alumina coating. The nozzle angle variation had a great influence on the reaction coating quality with the best coating results being achieved when the nozzle angle was at 55°. Therefore, the Ti PVD pre-coating and 55° nozzle angle were chosen for all of the later laser-induced reaction alumina coating experiments.

In order to obtain a set of optimum process parameters, laser-induced reaction alumina coating tracks were produced using the range of laser processing parameters given in Table 4-1. Various resulting features were investigated such as surface quality, transformation of aluminum, topography, microstructure and phase formation. The observations showed that an effective coating (smooth, pore free and good bonding)

Table 4-1 Laser Processing Parameters Used During Laser Induced Reaction Coating of Ceramics with Dynamic Fluidized Bed Powder Feeder

Trial #	Powder Feeder Flow Meter Reading (mm)		Argon Flow Meter Reading (shield gas) (mm)	Laser Power (watts)	Traverse Speed (mm/min)	Focal Position above the Sample Surface (mm)	Overlap (%)	Laser Beam Diameter (mm)	Remarks
	Air	O_2							
1	40	0	20	500	1800	5	56	0.67	no breaks, coarse metal coating.
2	30	0	20	500	1800	5	37	0.67	broke into two pieces, coarse metal coating.
3	30	10	0	500	1800	5	37	0.67	no breaks, coarse metal coating.
4	30	10	0	500	1800	5	37	0.67	no breaks, broke when remelted. coarse metal coating
5	25	20	0	400	1800	5	37	0.67	no breaks, coarse metal coating
6	25	20	0	300	1800	5	37	0.67	no breaks, coarse metal coating
7	25	20	0	300	1800	5	37	0.67	no breaks, coarse metal coating
8	25	20	0	300	1800	5	37	0.67	no breaks, coarse metal coating
9	25	20	0	300	1800	5	37	0.67	no breaks, coarse metal coating
10	25	35	0	300	1800	5	37	0.67	no breaks, coarse metal coating
11	25	50	0	300	1800	5	37	0.67	no breaks, coarse metal coating
12	25	50	0	300	1800	5	37	0.67	no breaks, coarse metal coating
13	25	35	0	200	1800	5	37	0.67	no breaks, fine metal coating
14	15	35	0	200	1800	5	37	0.67	no breaks, fine metal coating
15	7.5	7.5	25	200	1800	5	37	0.67	no breaks, fine metal coating
16	0	10	25	150	1800	5	37	0.67	no breaks, fine metal coating
17	0	10	25	250	1800	5	37	0.67	no breaks, fine metal coating
18	0	10	25	250	1800	10	38	1.33	broke into three pieces, smooth alumina coating
19	0	20	25	250	1800	10	38	1.33	broke into many pieces, smooth alumina coating
20	0	20	10	250	1800	10	38	1.33	broke into three pieces, smooth alumina coating

Table 4-1 Continued

Trial #	Powder Feeder Flow Meter Reading (mm) Air	O_2	Argon Flow Meter Reading (shield gas) (mm)	Laser Power (watts)	Traverse Speed (mm/min)	Focal Position above the Sample Surface (mm)	Overlap (mm) (%)	Laser Beam Diameter (mm)	Remarks
21	0	15	10	220	1800	10	38	1.33	break into two pieces, smooth alumina coating
22	0	15	10	225	1500	10	38	1.33	broke into two pieces, smooth alumina coating
23	0	15	10	225	1200	10	38	1.33	broke into many pieces, smooth alumina coating
24	0	15	10	225	2000	10	38	1.33	broke into three pieces, smooth alumina coating
25	0	15	10	300	1800	10	38	1.33	broke into three pieces, smooth alumina coating
26	0	15	10	200	1800	8	38	1.33	broke into two pieces, fine beard coating
27	0	15	10	150	1800	8	47	1.07	no breaks, smooth alumina coating
28	0	15	10	150	1800	8	40	1.07	no breaks, smooth alumina coating
29	0	15	10	150	1800	8	40	1.07	no breaks, smooth alumina coating
30	0	15	10	150	1800	8	40	1.07	no breaks, smooth alumina coating
31	0	15	10	150	1800	8	40	1.07	no breaks, smooth alumina coating

could be achieved within a selective range of the laser process parameters. It indicated that the complete laser-induced reaction alumina coating (the aluminum powder was completely oxidized into alumina) could be obtained only when the aluminum powder was delivered by pure oxygen gas. This results in very low laser power needed for the reaction coating.

Figure 4-1 shows an overview of the samples from trial 1 to 31. Figure 4-2 is a higher magnification view of some of the samples in Figure 4-1. Figure 4-3 is a high magnification view of Figure 4-2 (c). It appeared that trials 27-31 produced an adherent, relatively smooth and crack-free coating of Al_2O_3 on the $SiC_{(P)}/Al_2O_3$ substrate surface and so their process parameters were considered as the optimum. The marked difference in the surface roughness of the as-received and the laser-induced alumina coating may be seen from comparing Figure 3-1(a) and Figure 4-3. Outside the optimum range, problems appeared such as: samples breaking during laser processing, a rough surface coating layer, metal beads forming on the surface, and incomplete aluminum transformation into alumina.

Although there were some microcracks within the coating as seen in Figure 4-3, these cracks are very shallow. Few of them penetrated further into the coatings or substrate as illustrated in Figure 4-4. The cross-sectional view shows a defect free interface and the coating appeared uniform with a limited amount porosity. The laser induced transformation of the aluminum into the ceramic coating was confirmed by using x-ray diffraction. Figure 4-5 shows the x-ray diffraction analysis of the laser-induced reaction transformed alumina coating on the $SiC_{(P)}/Al_2O_3$ substrate.

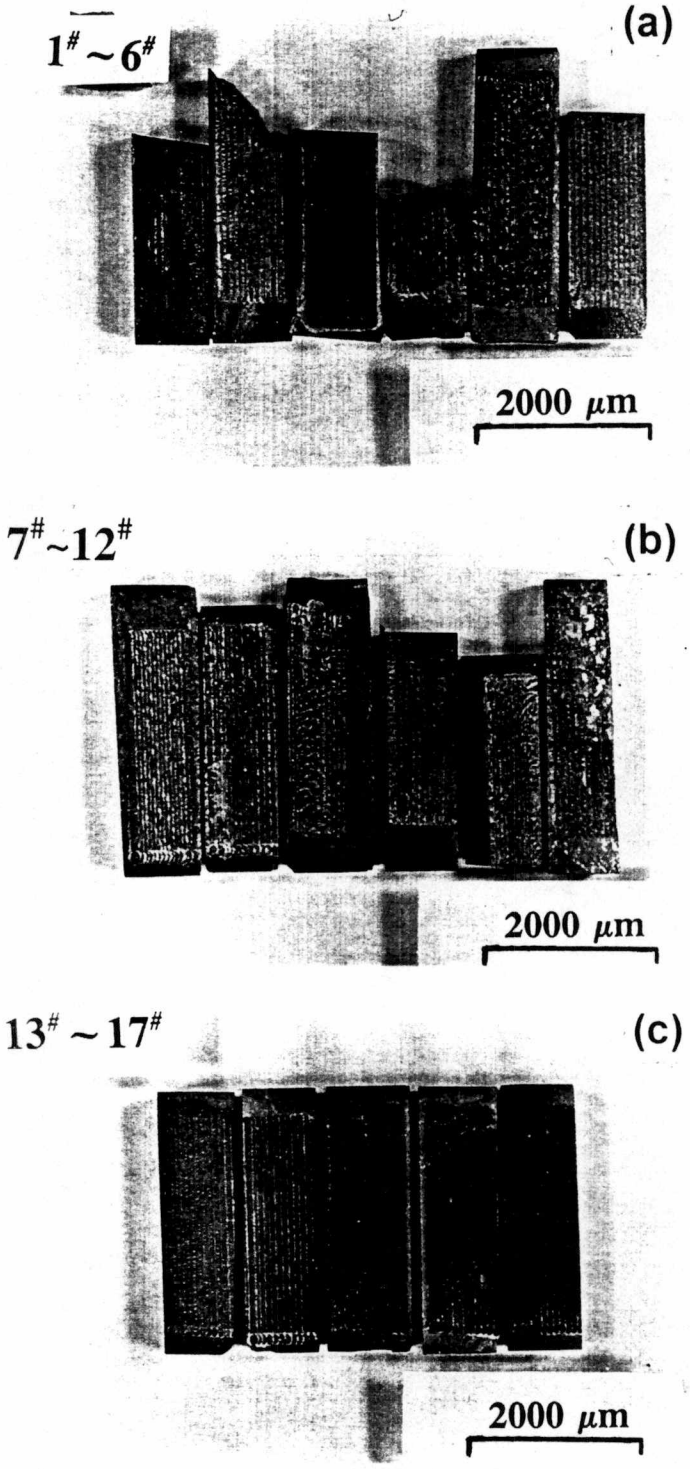

Figure 4-1. Overviews of topographical features of a laser-induced alumina coating on $SiC_{(P)}$/ Al_2O_3 composite samples. [(a)~(c) samples from trials #1 to #17]

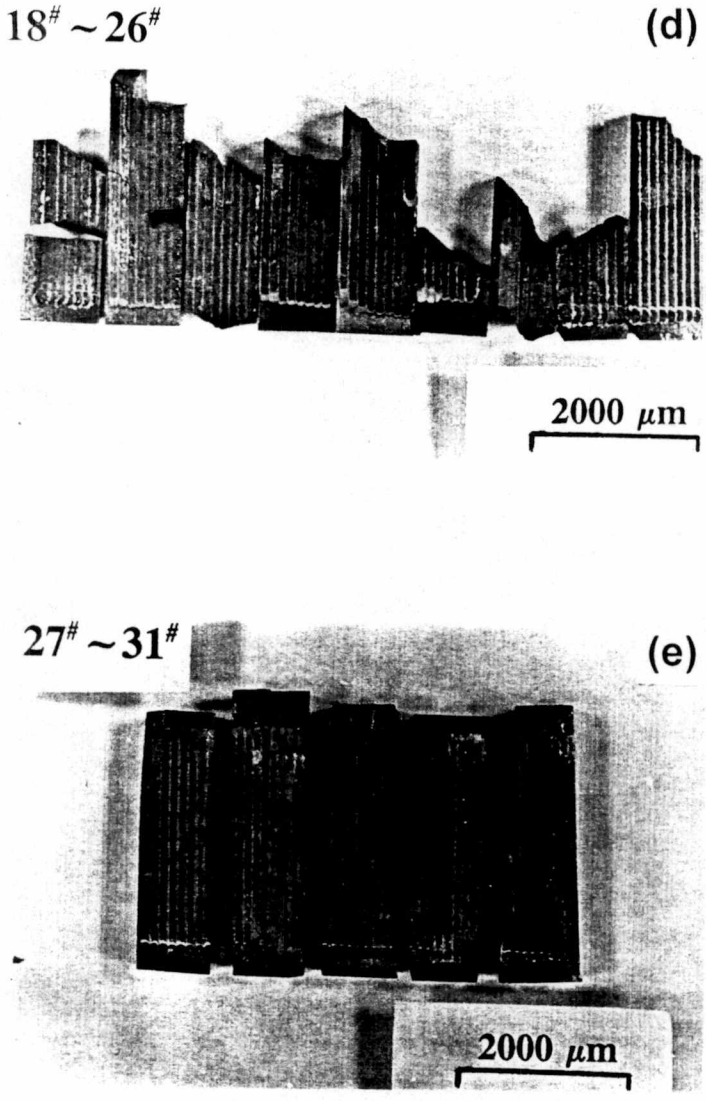

Figure 4-1 continued: Overviews of topographical features of a laser-induced alumina coating on $SiC_{(P)}$/ Al_2O_3 composite samples. [(d)~(e) samples from trials #18 to #31]

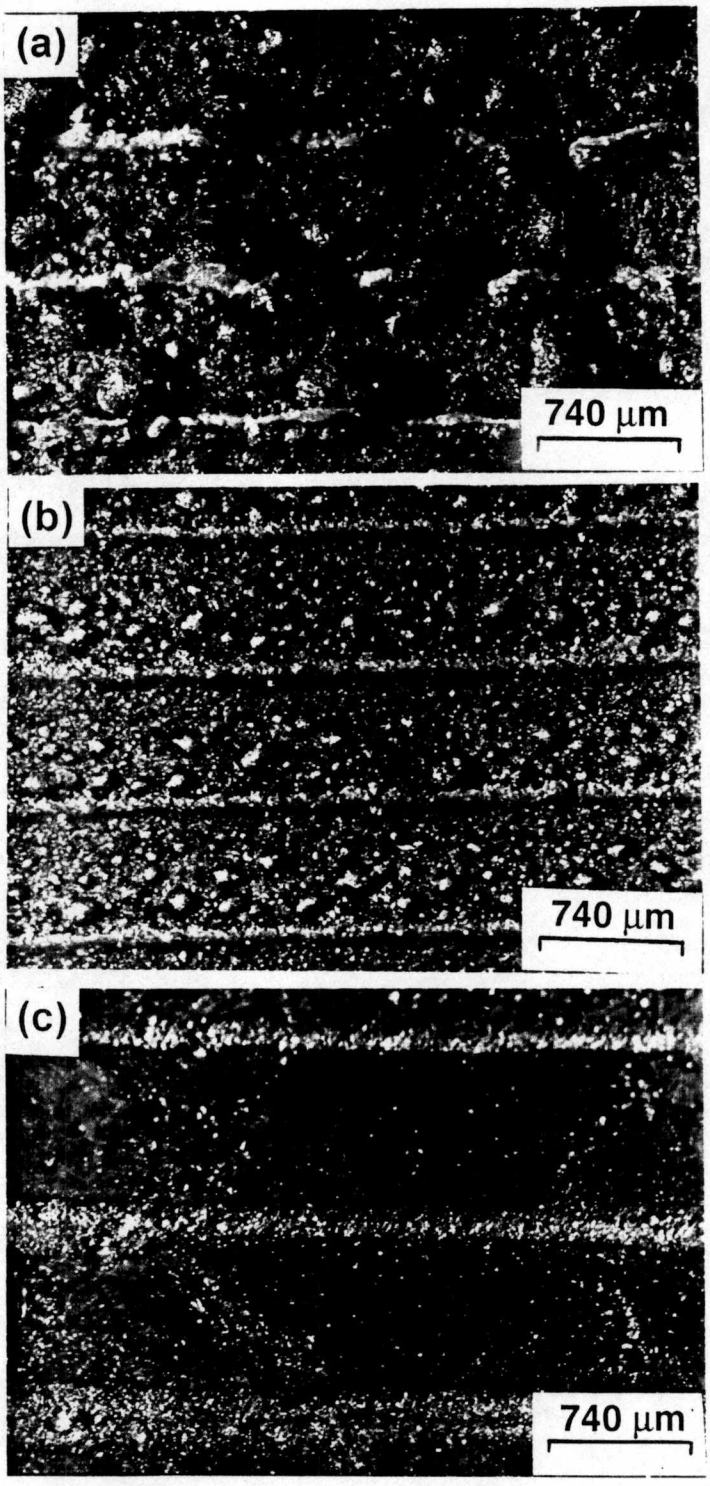

Figure 4-2 Magnified views of some samples in the Figure 4-1. [(a) trial #8, (b) trial #17 and (c) trial #28.]

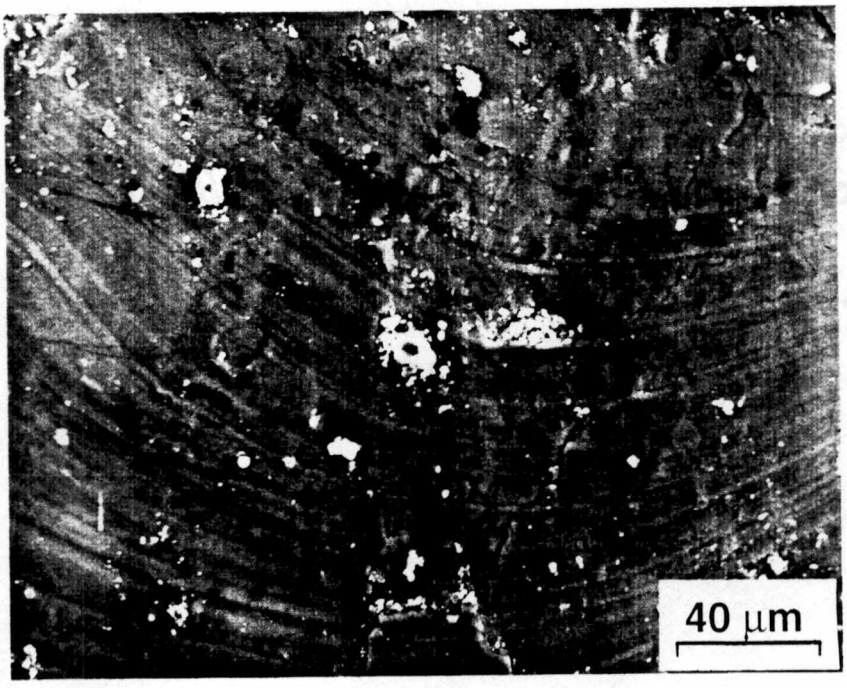

Figure 4-3 SEM photograph of a high magnification view for the sample from trial #28.

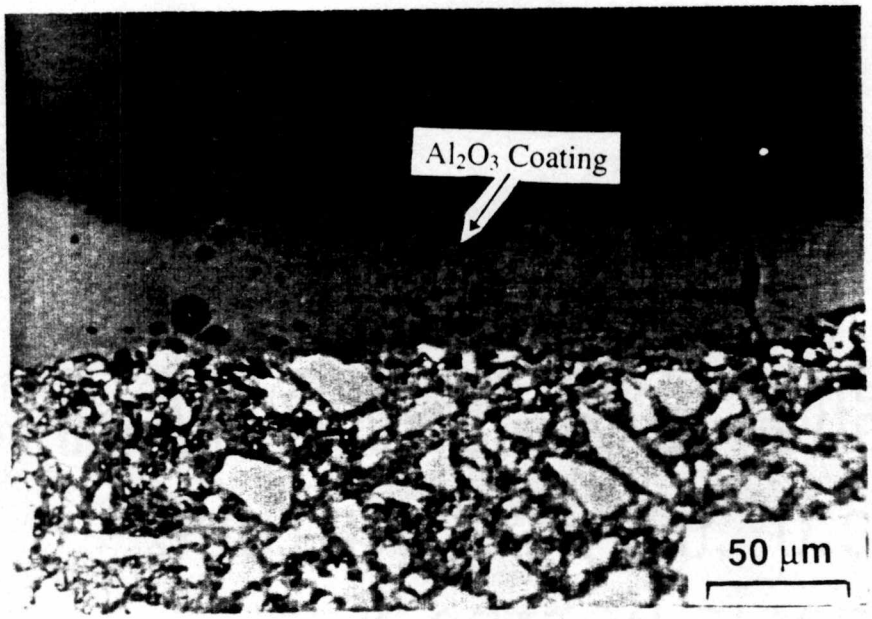

Figure 4-4. Cross-sectional view of the laser-induced reaction-coated $SiC_{(P)}/Al_2O_3$

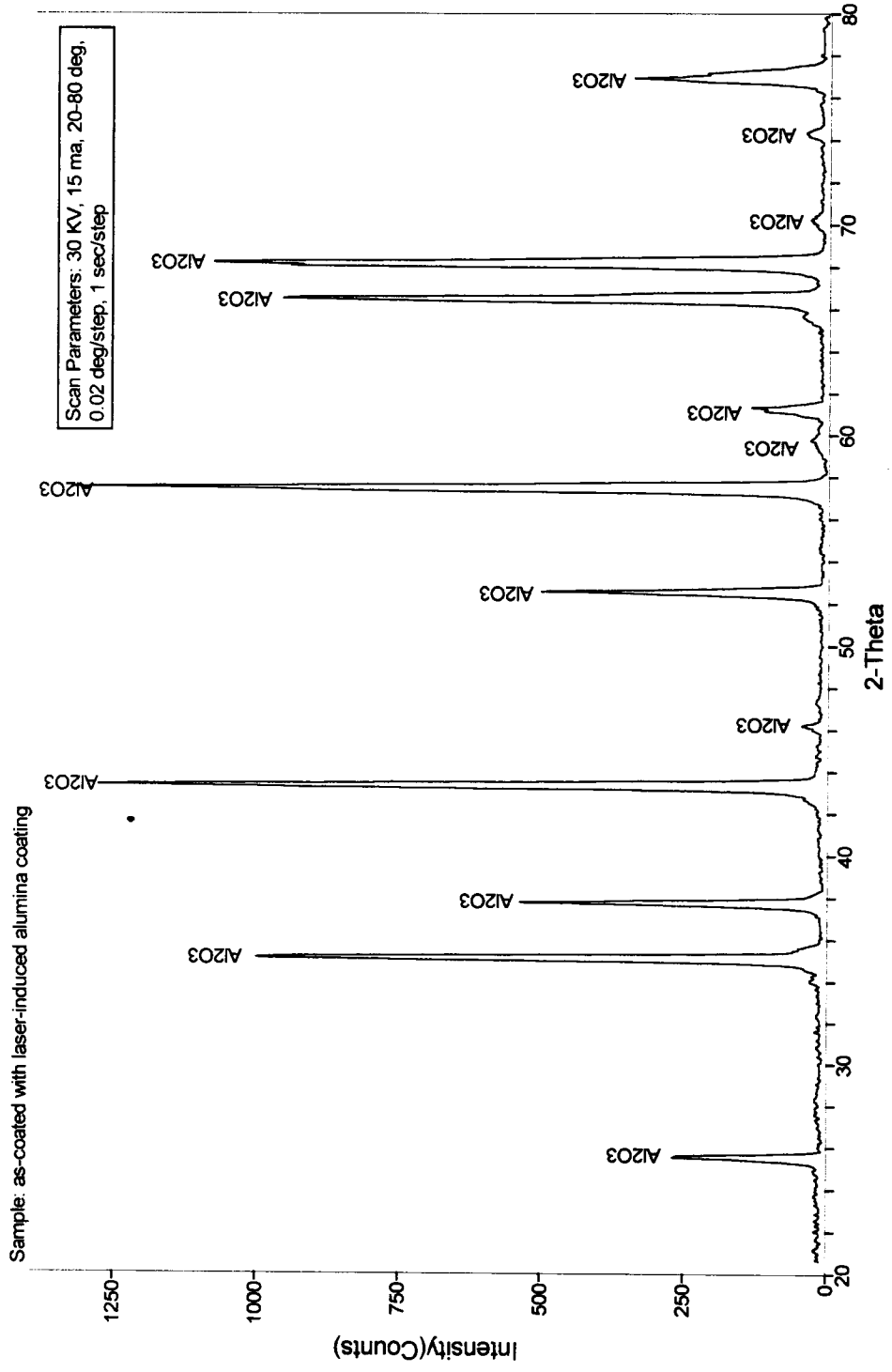

Figure 4-5. X-ray diffraction analysis of laser-induced reaction-coated $SiC_{(P)}/Al_2O_3$ (a scan of the coating)

The x-ray pattern indicates the existence of Al_2O_3 peaks and the absence of any other phase within the sensitivity of the instrument.

Rippling effects on the surface of the laser coating were observed as illustrated in Figure 4-3. The main rippling effect is perpendicular to the traverse direction. Similar features (often called chevrons) have been studied in detail by various researchers [83-84] for a variety of metallic alloys subjected to laser surface melting. The phenomena involved are complex, and depend on the surface tension driven flow and the resonant wave length of the melt pool. and is essentially a function of the temperature dependence of the surface tension. This may explain the differences between the rippling in laser melted metals and the laser coated ceramics. The ripples in metals have a herring bone formation with respect to the traverse direction, whereas, in the case of the laser ceramics coating, they are nearly perpendicular. This may be a consequence of the low thermal conductivity of the ceramic and the fact that, unlike most metals, the conductivity of alumina is effectively invariant with temperature. These characteristics of the conductivity will affect the temperature gradient, and hence surface tension differences.[85]

Initially the aluminum and titanium bond layer was deposited using the PVD (physical vapor deposition) technique because this nanoscale particle layer provides a strong interface via formation of reaction products (phases) with the base ceramic. It also provides a resilient metallic buffer zone to the very high thermal stresses developed between the ceramic substrate and the ceramic coating during the laser-induced reaction treatment. The absence of surface cracks and the strong adherence of the coating

indicate that both bond coatings have served their purpose in the present case. In practice, wetting may also be improved by adding other reactive elements, especially titanium. The beneficial effects of reactive additives on wettability have been mainly addressed as due to a reduction of interface energy. It was observed in this study that the titanium bond coat provided better wettability than the aluminum bond coat.

The formation of Al_2O_3 during laser treatment in an oxygen atmosphere primarily occurs according to the following reaction:

$$4Al\ (l) + 3O_2\ (g) \rightarrow 2Al_2O_3\ (s) \qquad (4\text{-}1)$$

The Gibbs free energy of the above reaction is:

$$\Delta G^\circ = -1{,}676{,}000 + 320T\ (J)\ \text{for}\ 973\text{-}1800K^{(86)}$$

where T is the temperature in K

The formation of Al_2O_3 in the above reaction can occur by either of two possible mechanisms: 1) self-diffusion of aluminum through a thin surface layer of alumina with oxidation occurring at the alumina-oxygen interface, or 2) diffusion of oxygen through a thin surface layer of alumina with the oxidation occurring at the alumina-aluminum interface. However, the diffusivity D_{Al}, for aluminum diffusion in alumina (9.48×10^{-15} cm^2/sec) is higher than the diffusivity for oxygen (D_{oxygen}) in alumina (4.4×10^{-18} cm^2/sec),[87] indicating that the aluminum transport dominates.

The initial supply of oxygen is such that other oxides in addition to Al_2O_3 also are formed via reactions of the type[88]

$$2M(alloy) + O_2\ (g) \rightarrow 2MO\ (s) \qquad (4\text{-}2)$$

where M indicates other metallic elements. So in order for the Al_2O_3 to form, the following additional reaction must be favorable:[89-90]

$$2Al\ (alloy) + 3MO \rightarrow Al_2O_3 + 3M\ (alloy) \qquad (4\text{-}3)$$

The amount of oxidation depends upon the composition of the alloy, the stability of the oxides formed, the growth rate of the oxide, and the diffusion of aluminum to the alloy-oxide interface. For Equation 4-3 to proceed, the standard free energy of formation of Al_2O_3 must be more negative than that of MO, and the activity of aluminum at the alloy-oxide interface should be large compared to the activity of M. In the present case, although the oxide of silicon or titanium is quite stable, Al_2O_3 is more stable than these oxides because it has a lower standard free energy of formation than SiO_2 and TiO_2. This warrants the formation of Al_2O_3 through precise control over processing parameters such as laser power and the powder feeder rate.

The formation of other possible undesirable products such as SiO_2, TiO_2 and Al_4C_3, due to the reaction between oxygen, aluminum, titanium, and $SiC_{(P)}/Al_2O_3$, is ruled out. The phase Al_2O_3 has a substantially lower free energy of formation than SiO_2 and TiO_2 over a full range of temperatures up to 1800°C,[91] which reduces the chances of the formation of SiO_2 and TiO_2 over Al_2O_3 (Figure 4-6). The possibility of the reaction

$$4Al(l) + 3SiC(s) \rightarrow Al_4C_3(s) + 3Si(s) \qquad (4\text{-}4)$$

between aluminum and SiC to form Al_4C_3 is ruled out, especially at high temperatures (>650°C), because SiC has a lower free energy of formation over the full range of temperatures up to 1600°C[91](Figure 4-7). These arguments are substantiated by the x-

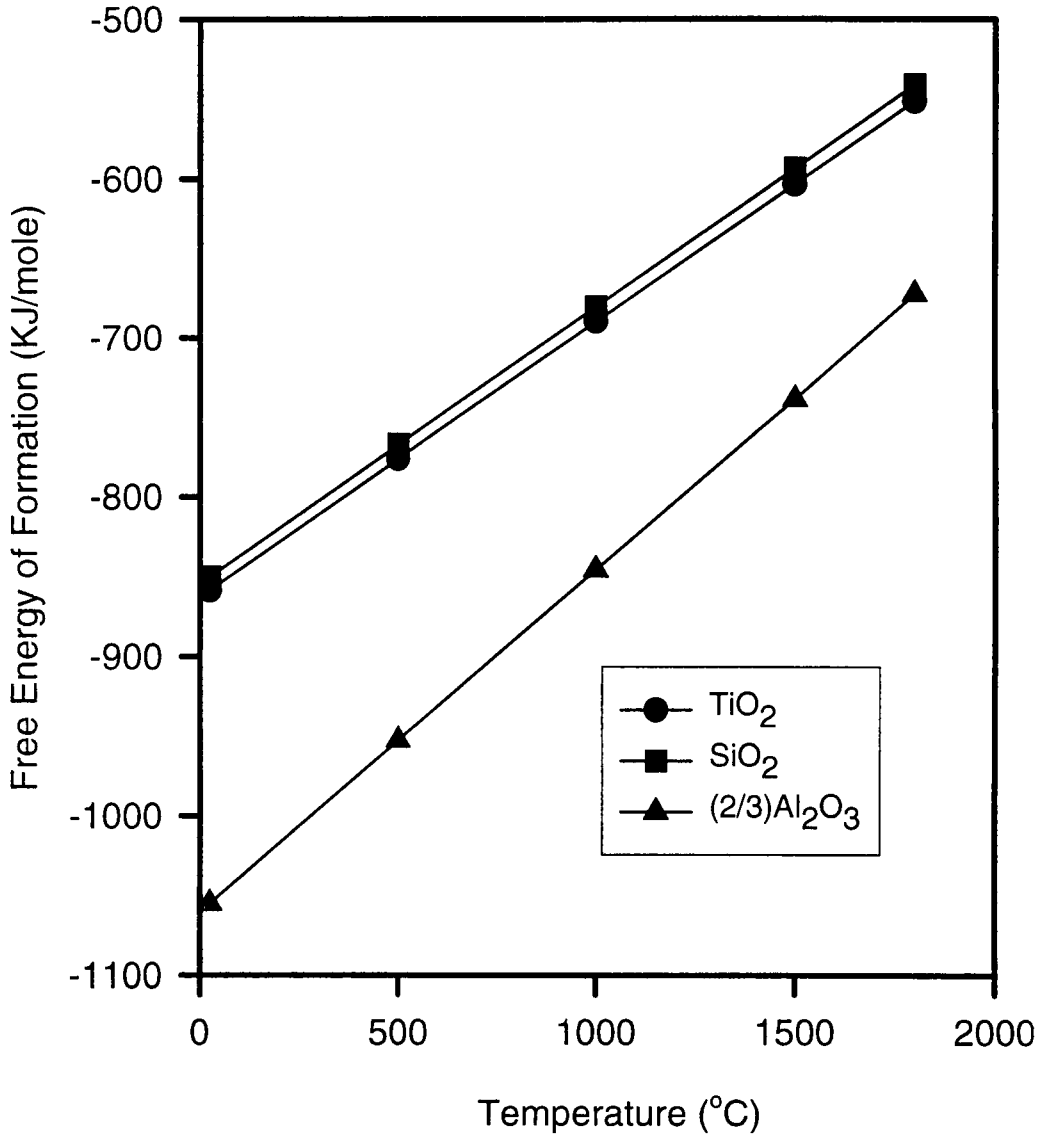

Figure 4-6. Free energy of formation as a function of temperature for SiO_2, TiO_2 and $(2/3)Al_2O_3$.

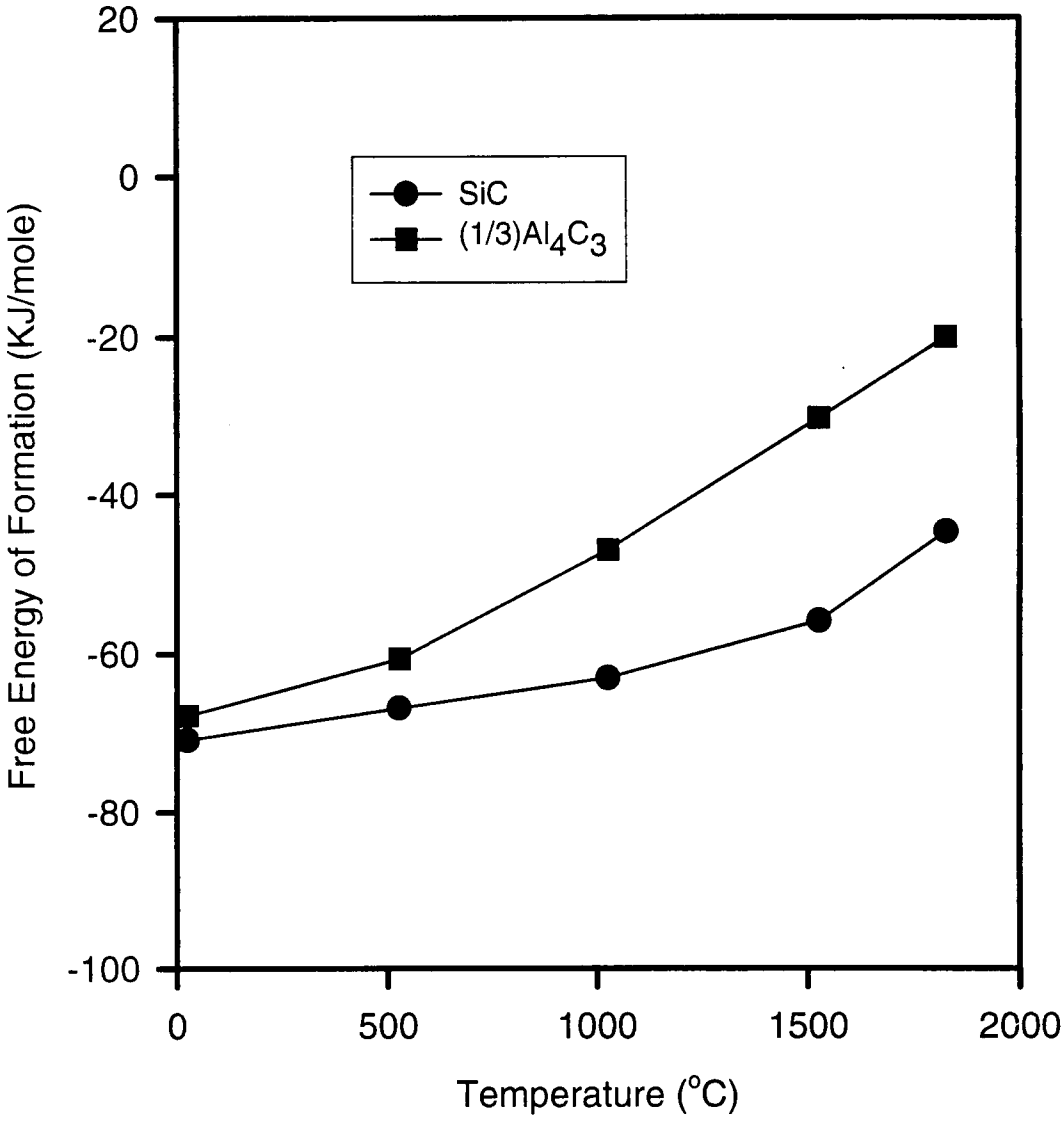

Figure 4-7. Free energy of formation as a function of temperature for SiC and $(1/3)Al_4C_3$.

ray diffraction analysis of the laser-induced reaction coated ceramic substrates (Figure 4-5), which showed the existence of only Al_2O_3 peaks.

4.2 Mechanical Testing

Table 4-2 and Table 4-3 present the mechanical testing results and Table 4-4 presents the summary of average values for the two sample sets. As seen in Table 4-4, a reduction of about 14% in the flexure strength (σ) of the laser coated sample compared to the as-received sample is realized. Such a reduction may be due to a single or combination of factors such as: thickness of the coating, physical characteristics (porosity and cracks) of the interface between the coating and the substrate, soundness of the coating (pores, cracks and inclusions), surface topography of the coating (roughness, cracks and pores) and chemical phases at the interface between the coating and the substrate. The evaluation of the relative strength provides a tool to choose a combination of materials and processing parameters at optimum levels for the production of sound and strong coatings.

Table 4-2. Three-Point Bending Test Results for the As-Received Samples

As-Received Samples			
Sample #	Fracture load P (lbs)	σ (Kpsi)	σ (MPa)
1	322	31.49	217.13
2	366	35.75	246.48
3	360	30.28	208.81
4	338	40.35	278.25
5	408	37.76	260.39
6	291	33.37	230.09
7	496	43.23	298.06
8	400	31.56	217.58
9	324	33.94	234.05
10	474	37.13	256.00
AVG.	378	35.49	244.68

Table 4-3. Three-Point Bending Test Results for the Laser Coated Samples

Laser Induced Reaction Coated Samples			
Sample #	Fracture load P (lbs)	σ (Kpsi)	σ (MPa)
1	275	28.84	198.83
2	315	28.90	199.26
3	381	40.27	277.67
4	468	37.97	261.78
5	422	32.50	224.09
6	294	25.72	177.32
7	288	27.30	188.23
8	288	25.98	179.15
9	323	28.85	198.89
10	286	27.23	187.74
AVG.	334	30.35	209.30

Table 4-4. Summary of Three-Point Bend Testing Results

	σ (Avg) (MPa)	StDev (Mpa)	Relative Value
As-received Samples	244.68	27.31	1
Laser-Induced Reaction Coating Samples	209.30	32.87	0.86

As mentioned in the manufacture's product catalogue, when a $SiC_{(p)}/Al_2O_3$ composite is heated to 1000~1500°C, its strength will reduce about 36% due to temperature (compared to the strength at room temperature)[92]. The study by Jon Winkler[66] indicated that the strength of the $SiC_{(p)}/Al_2O_3$ composite was degraded by 24% after the composite was exposed in the MHD furnace at 1150°C for 107 hours. The research by Peter LaRue[67] showed that the strength of the $SiC_{(p)}/Al_2O_3$ composite was degraded by 30~65% after the composite was exposed at 1100, 1260 and 1400°C with slag for 200 hours (the mechanical strength was also measured at 1100, 1260 and

1400°C). Research conducted by Breder and Parten[93] indicated that the strength of the $SiC_{(p)}/Al_2O_3$ was degraded by 25% after the composite was exposed at 1260°C with slag for 500 hours (the mechanical strength was measured at 1260°C). These reductions in strength mentioned to be due to corrosion effects on the samples during their exposure to high temperature corrosion environments. On the contrary in the present study, the bending tests showed only 14% reduction of strength after laser-induced reaction alumina coating. In view of this, if the coating provided corrosion protection for the composite, the relatively less reduction of strength (14%) is acceptable compared to the strength loss due to corrosion.

4.3 Corrosion of $SiC_{(P)}/Al_2O_3$ Composite

Figure 4-8 shows the changes in weight for the composite specimens with and without a laser-induced reaction alumina coating after 50, 100, 150, and 200 hours of exposure at 1200°C to a Na_2O_3 layer. Each data point represents the mean values of two test specimens. The samples were soaked in a HF water solution to remove Na-based corrosion products (silicates) prior to weight change measurement. All of the specimens exhibited an increase in weight. The samples without the laser-induced reaction alumina coating gained 30~32 mg/cm^2, while the laser-induced reaction alumina coated samples experienced marginal increase in weight, only 7.8~9.3 mg/cm^2. Note that there was no significant effect of exposure time on the weight change from 50 to 200 hours. This may be due to the limited amount of residual Aluminum in the Composite.

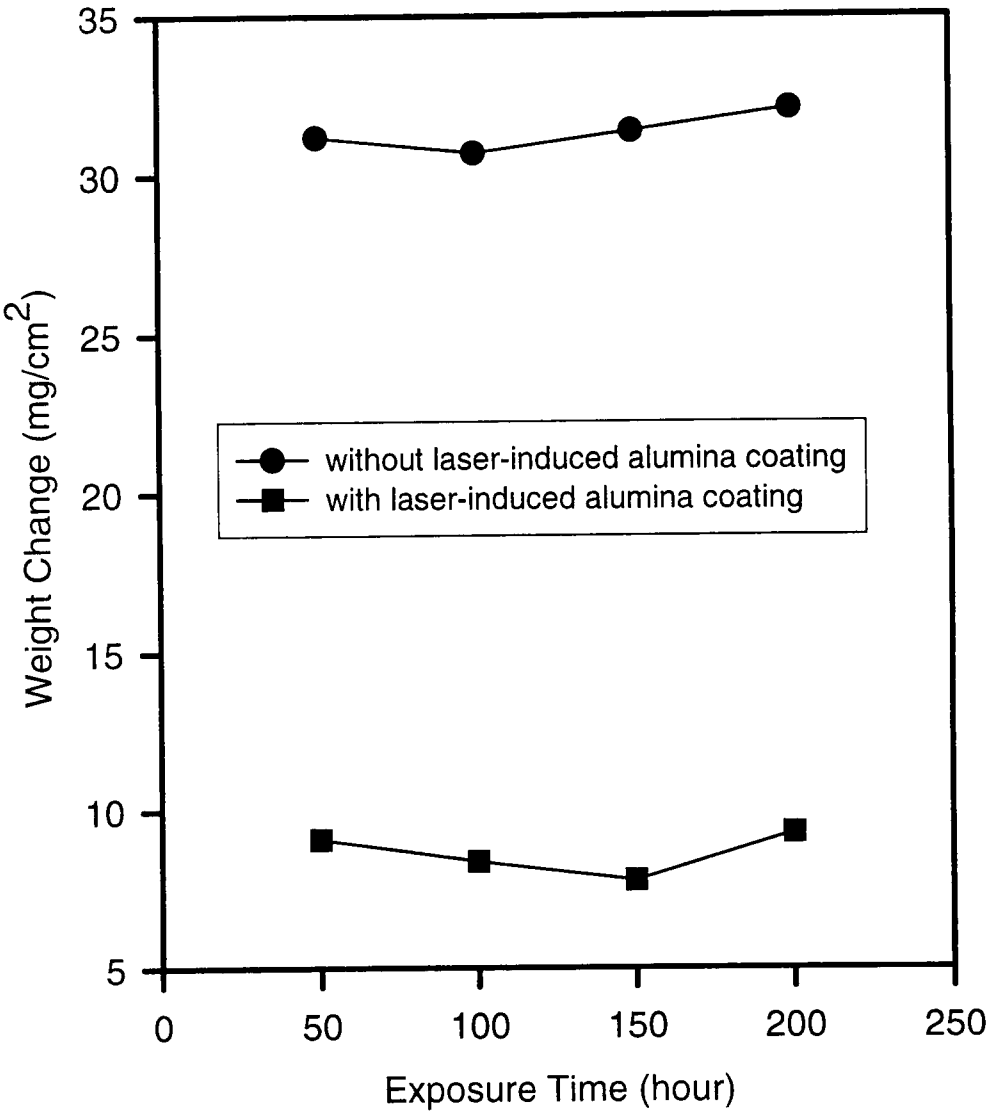

Figure 4-8 Weight change of SiC_P/Al_2O_3 composite specimens after exposure at 1200°C to a Na_2O_3 layer (after the corrosion products were removed by a HF solution).

A. Corrosion of the SiC_P/Al_2O_3 Composite without the Laser-induced Reaction Alumina Coating

The increase in weight of the non-coated specimens was due to the growth of a Si/Al_2O_3 oxidation product which had a morphology very similar to that of the matrix of the composite itself. Figure 4-9 is an optical microphotograph of the surface region of a specimen which had been exposed at 1200°C with a Na_2CO_3 layer for 150 hours. It appears that the oxidation product in the upper portion of the Figure 4-9 differs from the original SiC_P/Al_2O_3 composite only because it does not contain SiC particulate. There are more white-bright particles on the top of the oxidation product layer and more pores on the bottom of the oxidation region (explained later). The source of aluminum for the oxidation process was apparently residual metal contained in the composite, and this oxidation can be thought of as an uncontrolled resumption of the liquid metal oxidation process by which the composites were originally fabricated.[61~63] The occurrence of such oxidation product depend on the prior history of the sample and can be explained by following possible mechanism.

The SiC_P/Al_2O_3 composite was made by the directed metal oxidation (DIMOX™) of a molten aluminum alloy through a porous SiC preform. The microstructure of this material consists of SiC particles surrounded by a matrix of continuously interconnected Al_2O_3 formed by the oxidation process and residual metal. The composite is approximately 45% SiC, 52% Al_2O_3 and 1.6% residual metal Al-alloy by volume. While the exact composition of the starting alloy is proprietary, it is a

Figure 4-9. Optical microphotograph of cross-sectional view of the SiC_P/Al_2O_3 composite corroded at 1200°C for 150 hours after silicates removed with a HF solution showing Si/Al_2O_3 oxidation product on surface.

hypereutectic aluminum- silicon alloy (to minimize reactions with SiC during fabrication) doped with magnesium and zinc to promote the directed metal oxidation. It is expected that the SiC in the composite along with the residual metal gives the material a high thermal conductivity, strength and toughness, while the interpenetrating Al_2O_3 skeleton provides corrosion resistance at high temperature.[94] In this study, it was found that the composite consists of four phases. Along with the SiC, Al_2O_3, and residual Al mentioned above, there exists another phase, Si. (Figure 4-10 shows the x-ray diffraction data for the as-received composite; it indicates the presence of a silicon phase).

Figure 4-11 is a phase diagram for the Al-Si system.[95] There are only two phases: α phase and β phase, at room temperature. The α phase is a solid solution of silicon in aluminum. At the eutectic temperature, 577°C, the maximum solubility of silicon in aluminum is 1.65wt%, and only 0.05wt% at room temperature. Since the solubility of silicon in the α phase is very low and the properties of the α phase are very similar to those of pure aluminum, it may be considered the same as the Al phase. The β phase is a solid solution of aluminum in silicon. Because the solubility of aluminum in the β phase is extremely low, the β phase may be considered as pure silicon. When the amount of silicon in the Al-Si alloy exceeds 12.6%, it becomes the hypereutectic composition. During the solidification of the hypereutectic Al-Si alloy, the first solidification phase is β, called initial or primary Si, at 577°C, eutectic (α+β) appears and usually the β in eutectic (α+β) is called eutectic Si. Because the residual aluminum

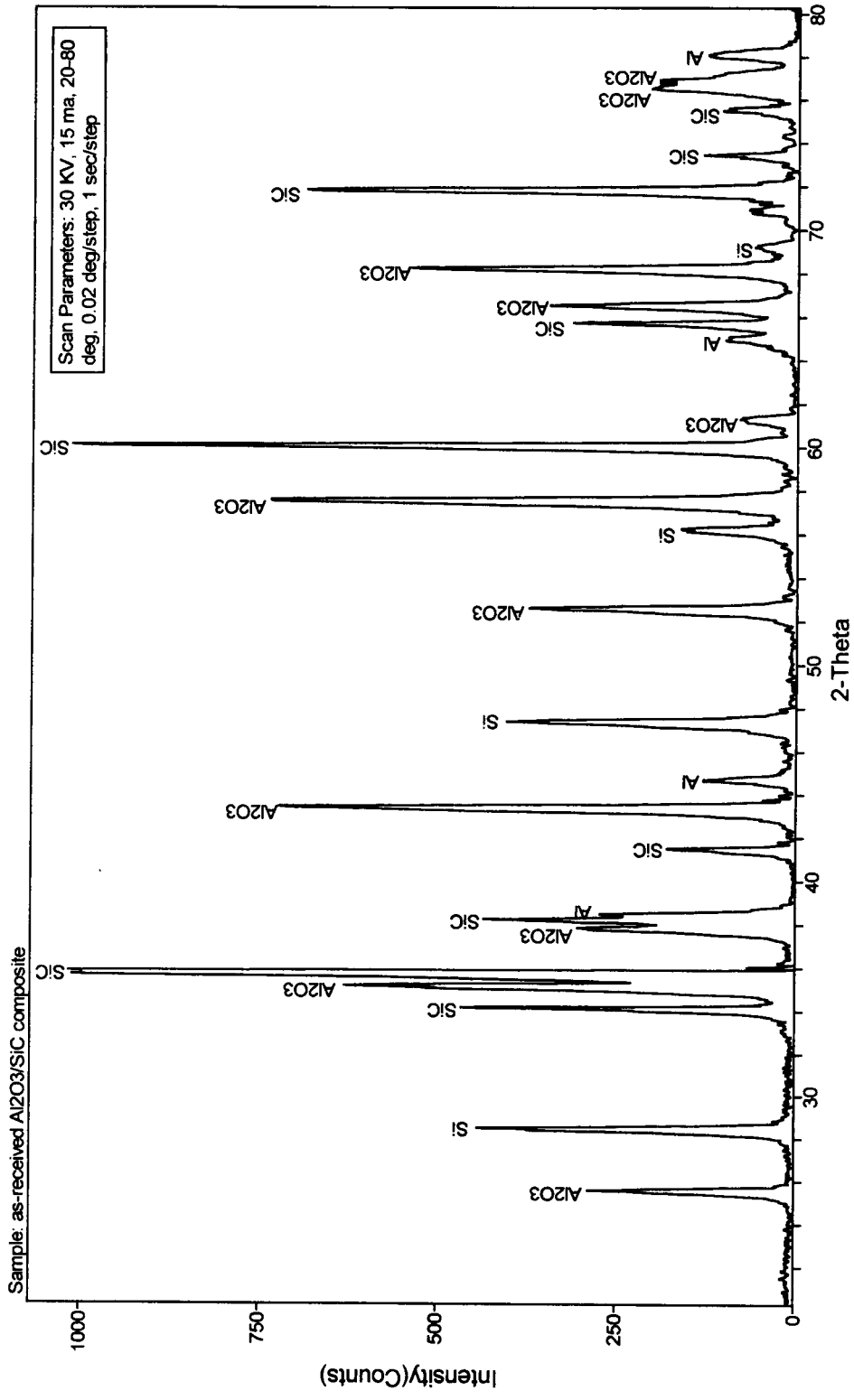

Figure 4-10. X-ray diffraction pattern of the as-received composite

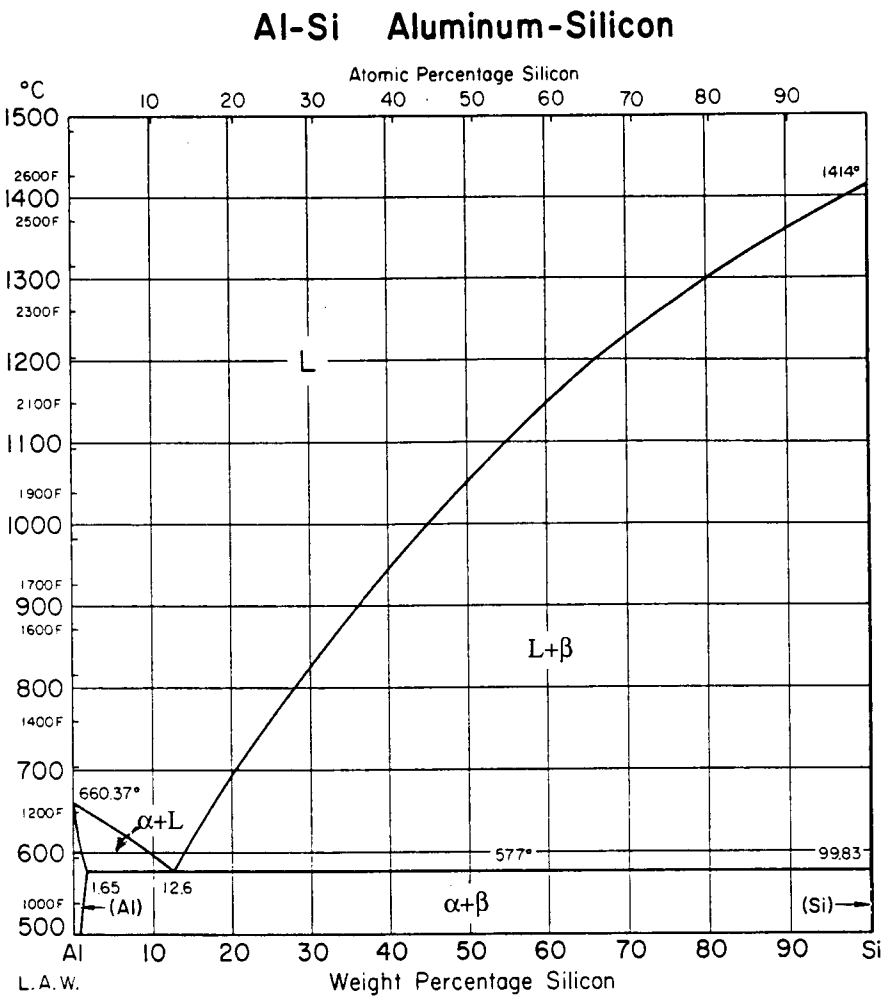

Figure 4-11. Al-Si phase diagram[95]

in the SiC_P/Al_2O_3 composite is the hypereutectic composition, there should be some silicon or β phase existing in the composite at the room temperature.

When the composite was exposed to high temperature, initially, some of the molten residual Al-Si alloy was drawn to the surface of the composite by capillary forces, but was not able to spread over the surface due to the relatively low surface energy. As the composite was further heated, the exposed SiC particles along with primary Si and /or β phase were oxidized to form a thin layer of SiO_2 causing an increase in the surface energy. Molten Al-Si alloy from the interior of the composite was then most likely drawn to the SiO_2, where it was able to spread over the surface and undergo rapid oxidation to form a solid Al_2O_3 thin film on the liquid metal surface. With an increase in exposure time, the oxidation film becomes thicker to form an oxidation layer and the silicon content in the residual liquid metal becomes richer. The growth direction of the oxidation product is from the inside surface to the outside surface of the composite. This indicates that the top of the oxidation layer has more Si than the bottom of the oxidation layer (refer to the Figure 4-9). The growth rate of the oxidation layer on the outside of the composite surface should depend on the extrusion rate of the molten liquid Al-alloy to the outer surface.

At the same time, in the wetting of the liquid Al on the SiO_2, the following chemical reaction occurred at their interface:

$$3SiO_2(s) + 4Al(l) \rightarrow 2Al_2O_3(s) + 3Si(s) \qquad (4\text{-}6)$$

(ΔG = -472 kJ/mol, 1200°C)

Based on this reaction, it results in the volume of the ceramic substrate being reduced by 38% from $3SiO_2$ to $2Al_2O_3$. In addition to this, following two more scenarios can be envisioned with relation to this reaction. If the Si formed from the reaction (Eq 4-6) becomes melted in the aluminum liquid (the solubility of Si in Aluminum is 67wt% at 1200°C) and if this liquid is then drawn to the surface of the composite during exposure, the volume of the substrate will be reduced by 58% from ($3SiO_2$ + 4Al) to $2Al_2O_3$. Even if all of the silicon stays at the original location, the volume is still reduced by 28% from ($3SiO_2$ + 4Al) to ($2Al_2O_3$ + 3Si). As a consequence, the Al_2O_3 grains formed in the substrate are separated by cavities along the boundaries due to the volume shrinkage. Some of the liquid metal would diffuse easily into these cavities. In front of the wetting triple line, surface cavities may be induced due to the shrinkage of the ceramics substrate during the reaction. This may hamper a further spreading of the liquid drop over the surface. Meanwhile, Al and the Si liquid alloy may diffuse to the surface cavities through the boundary cavities of the Al_2O_3 grains. A further reaction will then occur in front of the triple line. In this way, the chemical reaction takes place on the surface of SiO_2 before the spreading of liquid metal and leaves the cavities on the surface of the SiC particles. Under this condition, the growth direction of the corrosion product, Si/Al_2O_3, is from the original surface of the composite to the inside of the composite. This indicates that the protective SiO_2 layer on the SiC is also removed by aluminum (Eq 4-6). The unprotected SiC is then attacked by the oxidizing atmosphere and molten salt. The growth rate of the oxidation layer inside the composite might depend on at the rates of two reactions: First is the oxidation of SiC particles to become

SiO_2. Second is the dissolution of SiO_2 through the reaction (Eq 4-6). It is obvious that the growth rate of the oxidation layer on the outside surface of the composite is faster than in the inside of the composite.

The chemical reaction (Eq 4-6) also explains why there was a much higher increase in porosity within the composite after it was exposed at high temperature since the reaction (Eg 4-6) can also occur at the inside of the composite. Jon Winkler[66] observed that the porosity increased from 1.95% (volume percent) in the as-received SiC_P/Al_2O_3 composite to 23.24% after the composite was exposed to a high temperature with coal slag. The residual aluminum in the as-received composite was only about 7.16%. If all the residual aluminum was drawn out from the composite, the porosity should not have been more than 10% for his experiment. In the present study, the initial residual aluminum was about 1.6%. The porosity increased from 1.4% for the as-received composite to 4.78% after exposure at 1200°C with a layer of Na_2CO_3 for 200 hours.

Part of the silicon produced through reaction (Eq 4-6) will be dissolved in the aluminum liquid until the liquid saturates with silicon. At 1200°C, the maximum solubility of silicon in aluminum is about 67wt%. The surplus silicon will precipitate out just like the initial Si.

Figure 4-12 shows x-ray diffraction patterns of the SiC_P/Al_2O_3 composite after exposure at 1200°C for different time increments (The specimens were washed with a HF solution prior to x-ray analysis). The diffraction patterns indicate that there is no residual

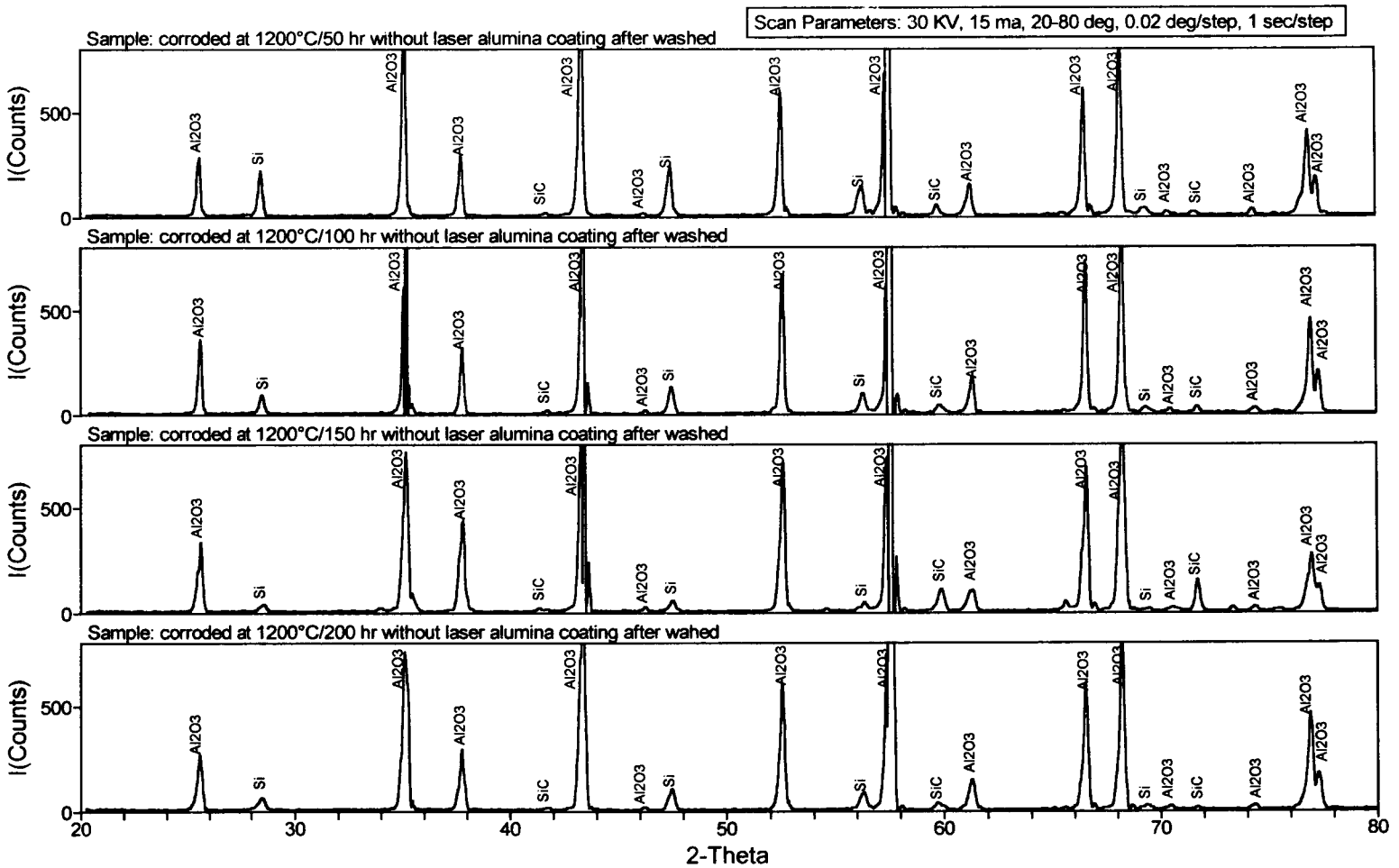

Figure 4-12. X-ray diffraction patterns of the specimens without the laser-induced reaction alumina coating after the corrosion products were removed with a HF solution

aluminum in the surface layer and all of the aluminum extruded from the substrate to the surface has been oxidized into Al_2O_3. There are minor amounts of Si and SiC existing in the oxidation layer. The presence of Si in the oxidation layer is consistent with the above discussion.

Figures 4-13 and 4-14 are cross-section SEM views of some corroded samples and their elemental x-ray maps. These pictures provide further proof concerning the existence of silicon and its distribution within the oxidation layer. Both Figure 4-13(d) and Figure 4-14(d) indicate that there is more silicon in both the top and the bottom of the oxidation layer than in the center of the layer. The elementary x-ray maps of Si in Figure 4-13 and Figure 4-14 also show that some of the SiC was attacked in the interface between the oxidation layer and the substrate composite as the interface is rough compared to the Si x-ray map in Figure 4-21 for the sample coated with the laser-induced reaction alumina coating.

Selective oxidation could result in selective corrosion. It is well known that SiC is resistant to oxidation because it forms a protective SiO_2 film. However, silica is soluble in basic salt melts according to the reaction :

$$SiO_2 + O^{-2} \rightarrow SiO_3^{-2} \qquad (4\text{-}7)$$

The growth of the oxidation layer was not uniform. There were regions on the surfaces where it was absent or very thin, and other regions where it was up to 300 μm thick. The areas where none or a thin Si/Al_2O_3 oxidation product formed were subject to corrosion by the sodium salt. Figure 4-15 is a cross-sectional microphotograph of the

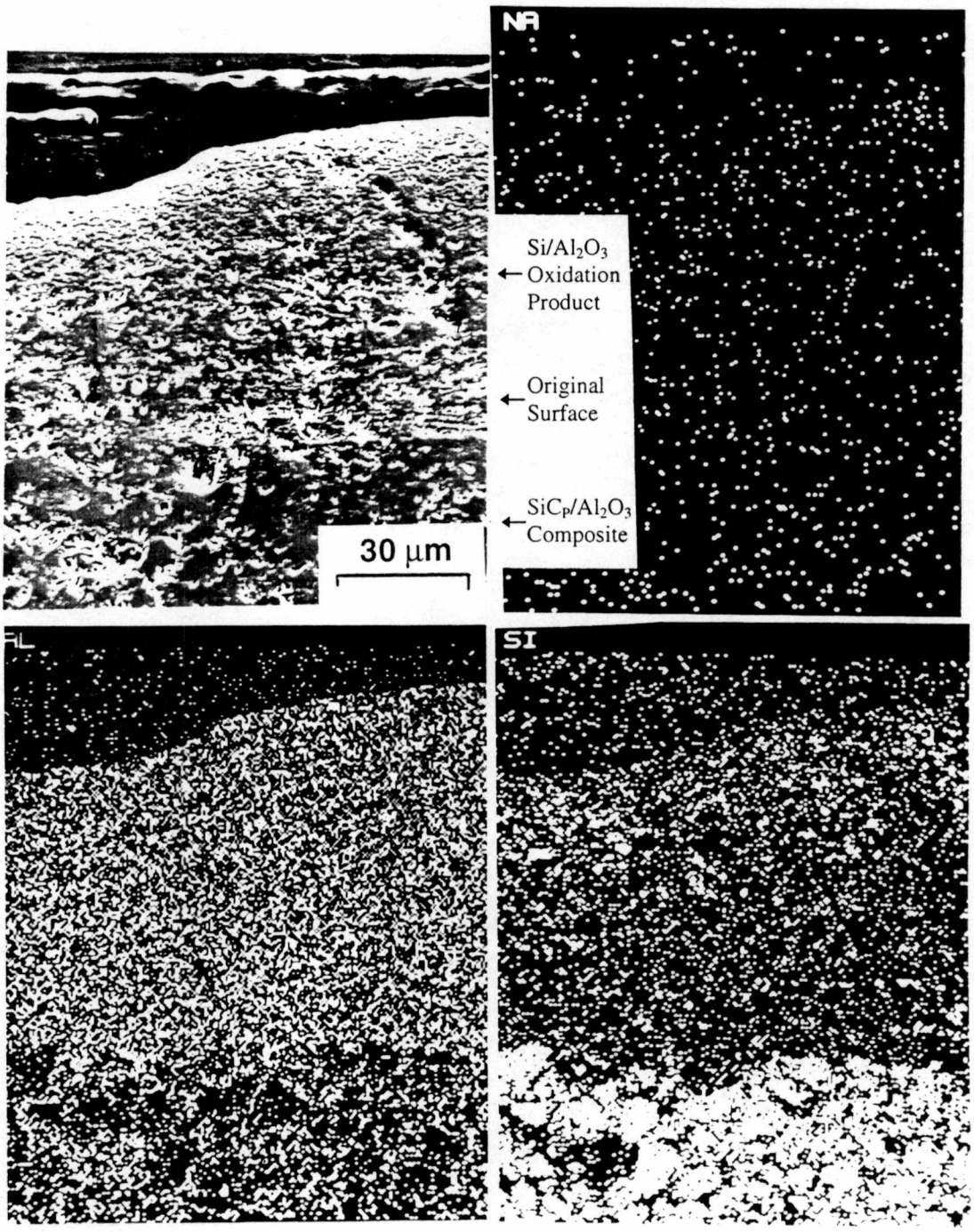

Figure 4-13. SEM photograph of a cross-sectional view and elemental x-ray maps of the SiC_P/Al_2O_3 composite corroded at 1200°C for 50 hours (silicates removed with a HF solution).

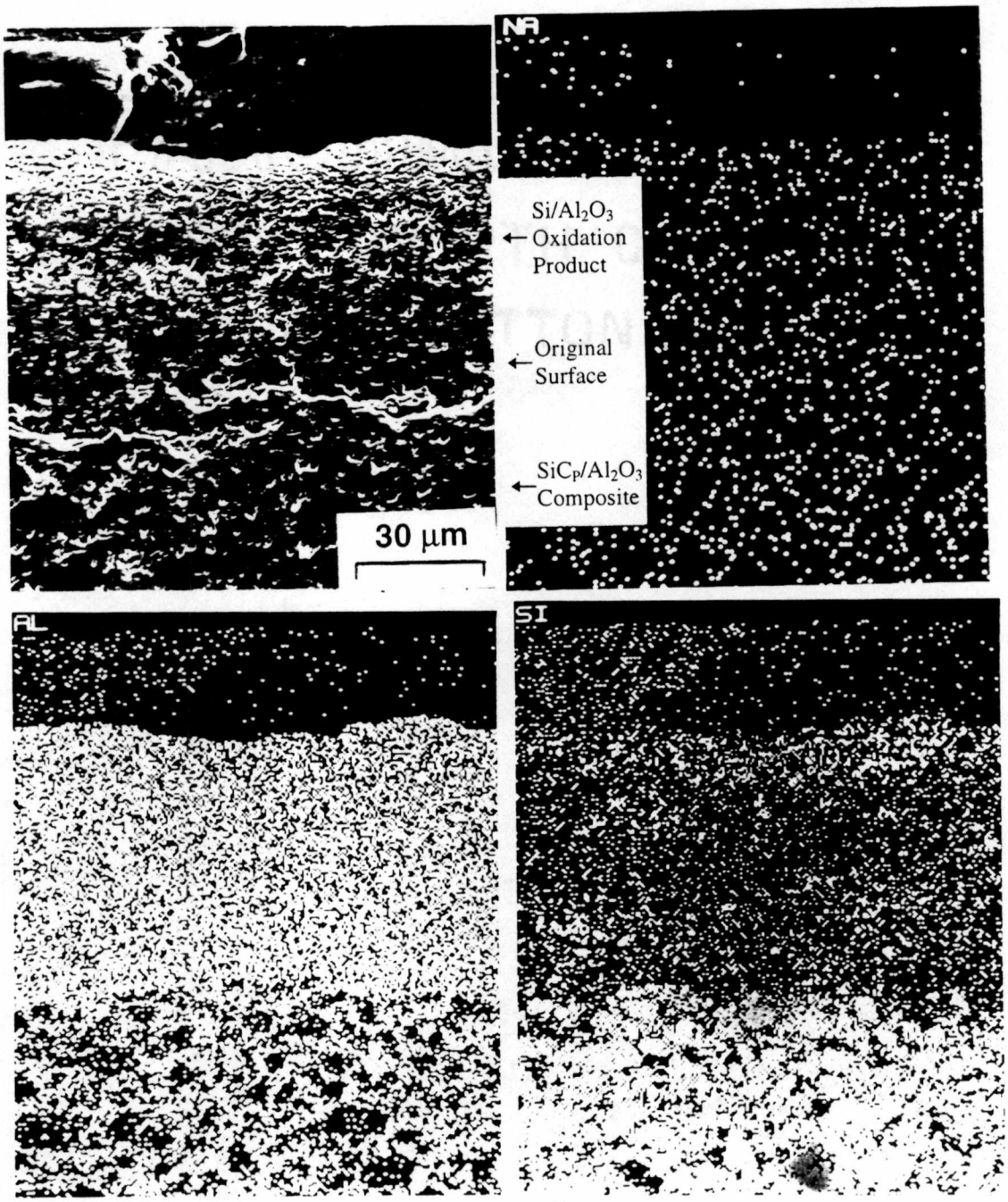

Figure 4-14. SEM photograph of a cross-sectional view and elemental x-ray maps of the SiC_P/Al_2O_3 composite corroded at 1200°C for 200 hours (silicates removed with a HF solution).

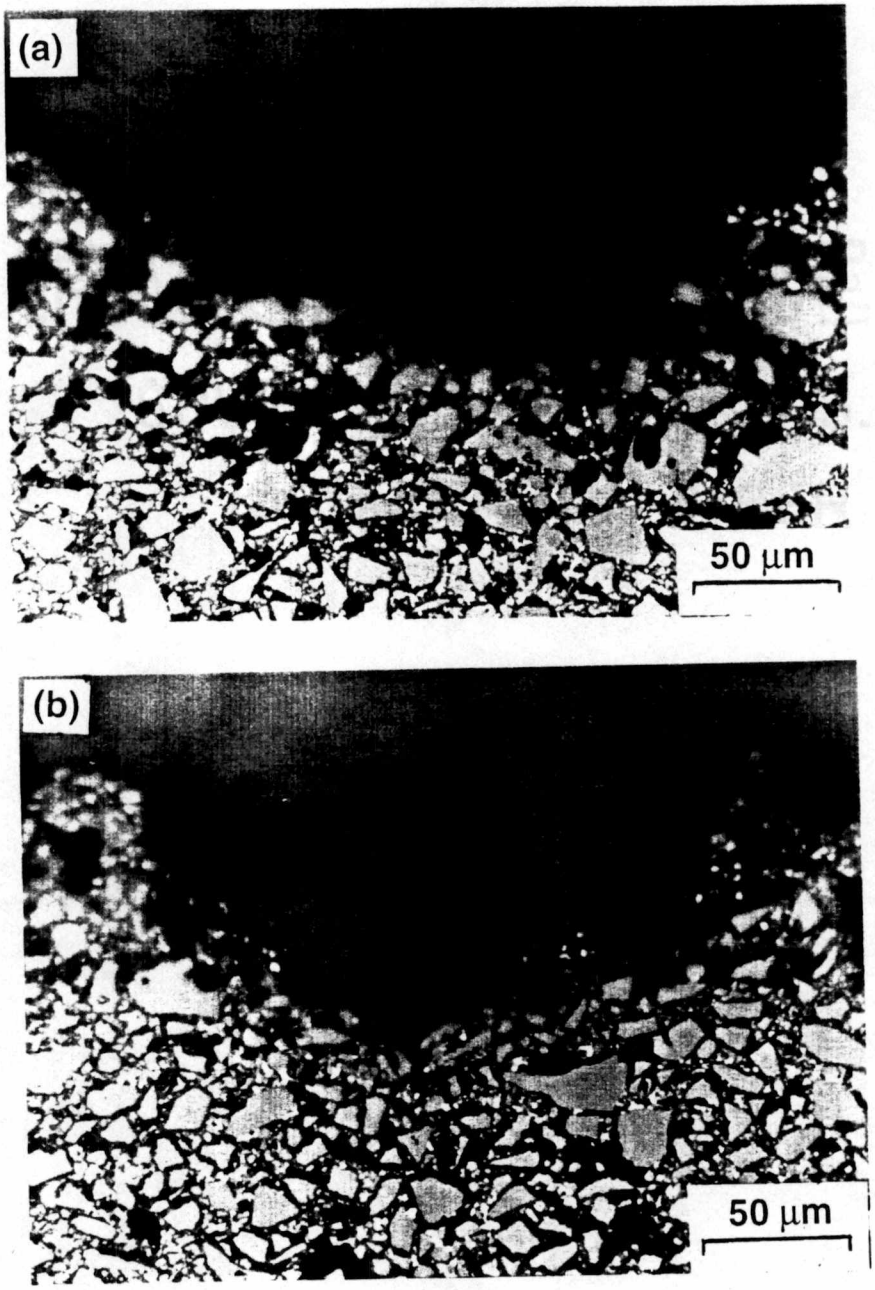

Figure 4-15. Optical microphotograph of a cross-sectional views for SiC_P/Al_2O_3 composite corroded at 1200°C after silicates removed with a HF solution. (a) for 50 hours, (b) for 200 hours

SiC_P/Al_2O_3 composite after 50 and 200 hours corrosion at 1200°C respectively. Corrosion of the composite is indicated by surface roughening and recession.

The corrosion begins with selective oxidation of the SiC particles on or near the surface (to form SiO_2) and the aluminum metal (to form Al_2O_3) in the composite followed by dissolution of the oxides in the molten salt. Because Al_2O_3 is generally regarded as much more corrosion resistant than SiC, the corrosion rate appears to controlled by the corrosion resistance of the Al_2O_3 matrix. There are some areas on the surface containing more SiC particles and less Al_2O_3 than other areas since the distribution of SiC particles is not uniform from a microcosmic view. Consequently, there was more SiO_2 formed in these local areas. In the presence of Na_2CO_3, SiO_2 can react directly with Na_2CO_3 melt to form low melting compound at exposure temperature:

$$Na_2CO_3\ (l) + xSiO_2\ (s) \rightarrow Na_2O{\cdot}xSiO_2\ (l) + CO_2\ (g) \qquad (4\text{-}8)$$

where x = 1 or 2

For x=2, the reaction product is $Na_2Si_2O_5$ whose melting point is 837°C.[96] $Na_2Si_2O_5$ can further react with Al_2O_3 to form a still lower melting eutectic $NaAlSiO_4$(1/2 $Na_2O{\cdot}Al_2O_3{\cdot}2SiO_2$) whose melting point is 760°C[97] according to following reaction:

$$Na_2O{\cdot}2SiO_2\ (l) + Al_2O_3\ (s) \rightarrow Na_2O{\cdot}Al_2O_3{\cdot}2SiO_2\ (l) \qquad (4\text{-}9)$$

Repeated oxidation and dissolution reactions at these local areas probably occur until all of the Na_2CO_3 is depleted. A characteristic feature of SiC corroded by alkali compounds is the presence of a previously molten silicate glass layer containing alkali oxides. Figure 4-16 shows some localized regions of the silicate glass layer which form

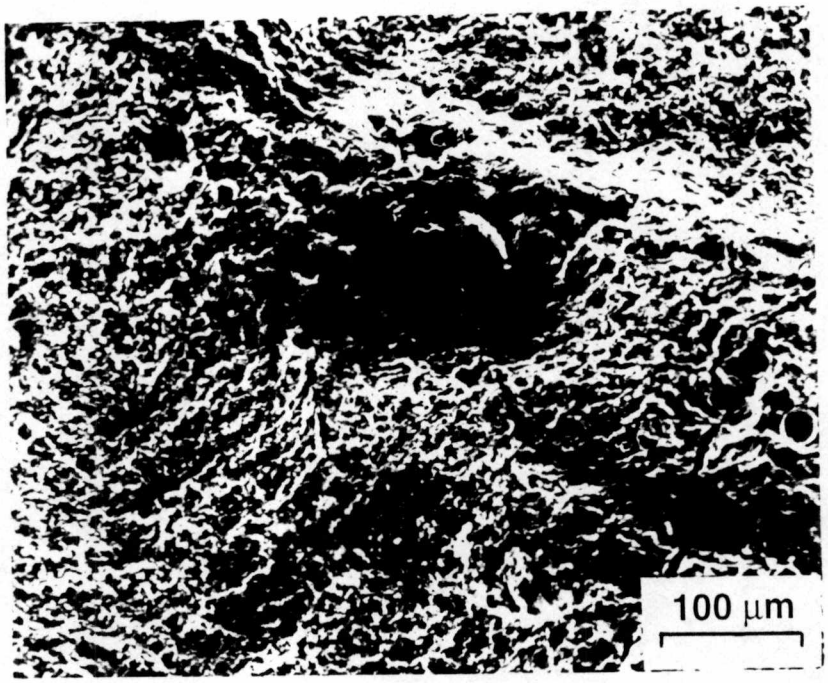

Figure 4-16. SEM photograph of surface view of specimen exposed at 1200°C for 50 hours showing glassy layer in center part (before the corrosion products were removed by a HF solution).

on the specimens. Figure 4-17 is a magnified view of the glassy area in Figure 4-16 and its elemental x-ray maps showing that the major constituent element is silicon. EDS analysis provides the composition of the glassy phase: 68.27 Si, 26.05 Al and 5.68 Na (by wt%). X-ray diffraction phase analysis also indicates that corrosion products contain some $Na_2Si_2O_5$, $NaAlSiO_4$, and $Na_2Al_{22}O_{34}$. The melting point of $Na_2Al_{22}O_{34}$ is more than 2000°C.[97] Figure 4-18 shows the x-ray diffraction patterns of the specimens before the corrosion products were removed by the HF solution. Figure 4-18 indicates that sodium silicates with a low melting point will disappear when the exposure time is increased. This may occur because these sodium silicates are liquids at the exposure temperature and they will flux away with time.

Figure 4-19 is a surface view of the structures underlying the glassy phase (glassy phase removed with a HF solution) and elemental x-ray maps. It also shows a localized pattern of attack on the surface. Some SiC particles were missing, leaving voids and some SiC particles were incompletely attacked due to the depleted Na_2CO_3 layer. This result is consistent with Figure 4-12 which indicated there was still some of the SiC phase existing on the surface of the specimens after the corrosion test.

B. Corrosion of SiC_P/Al_2O_3 Composite with Laser-induced Reaction Alumina Coating

The weight change for the composite with the laser-induced reaction alumina coating after exposure at 1200°C for 50, 100, 150 and 200 hours is shown in Figure 4-8. Each data point for the coated samples is based on the mean values of two test

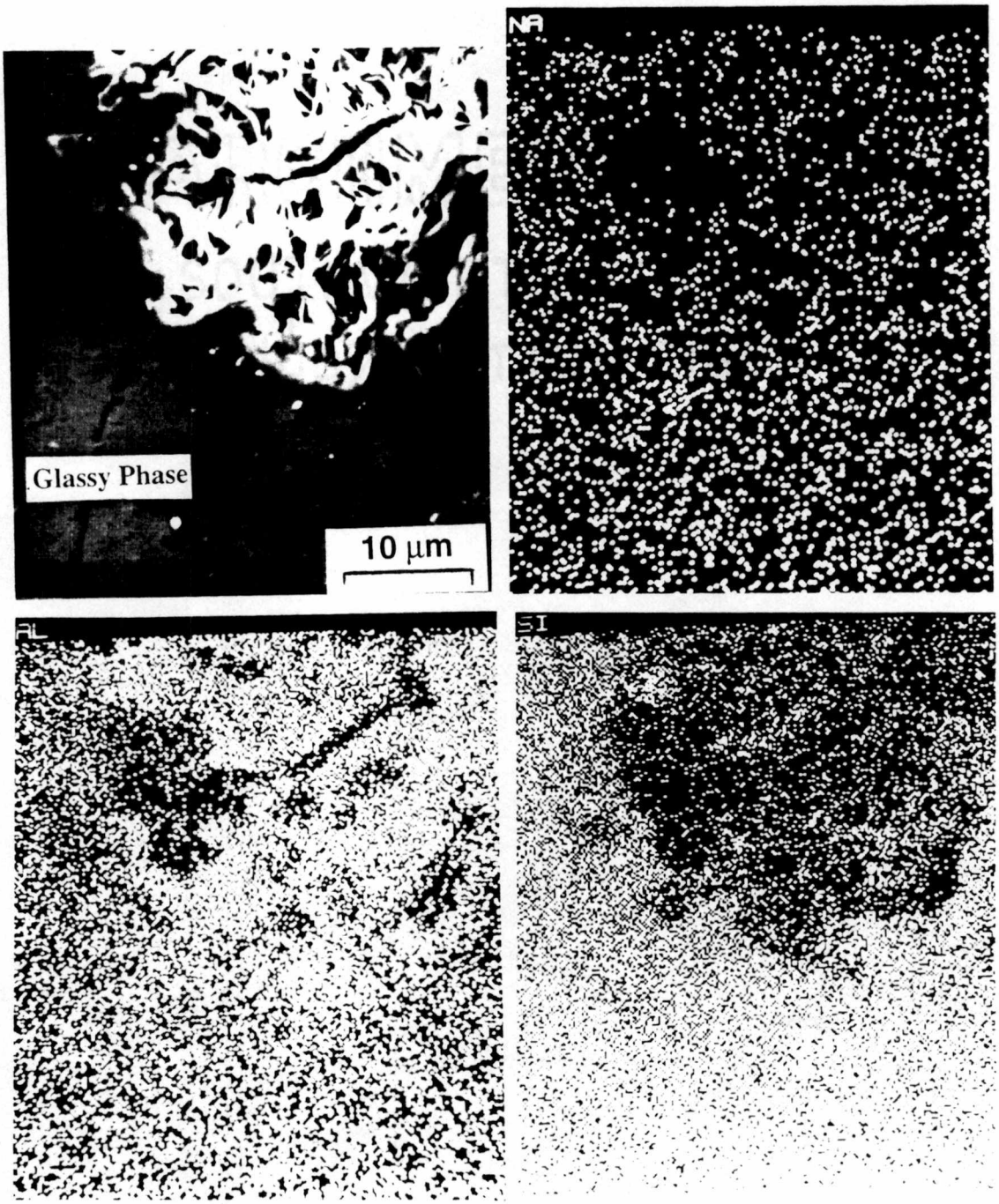

Figure 4-17. SEM photograph of magnified view of the glassy area shown in Figure 4-16 and its elemental x-ray maps

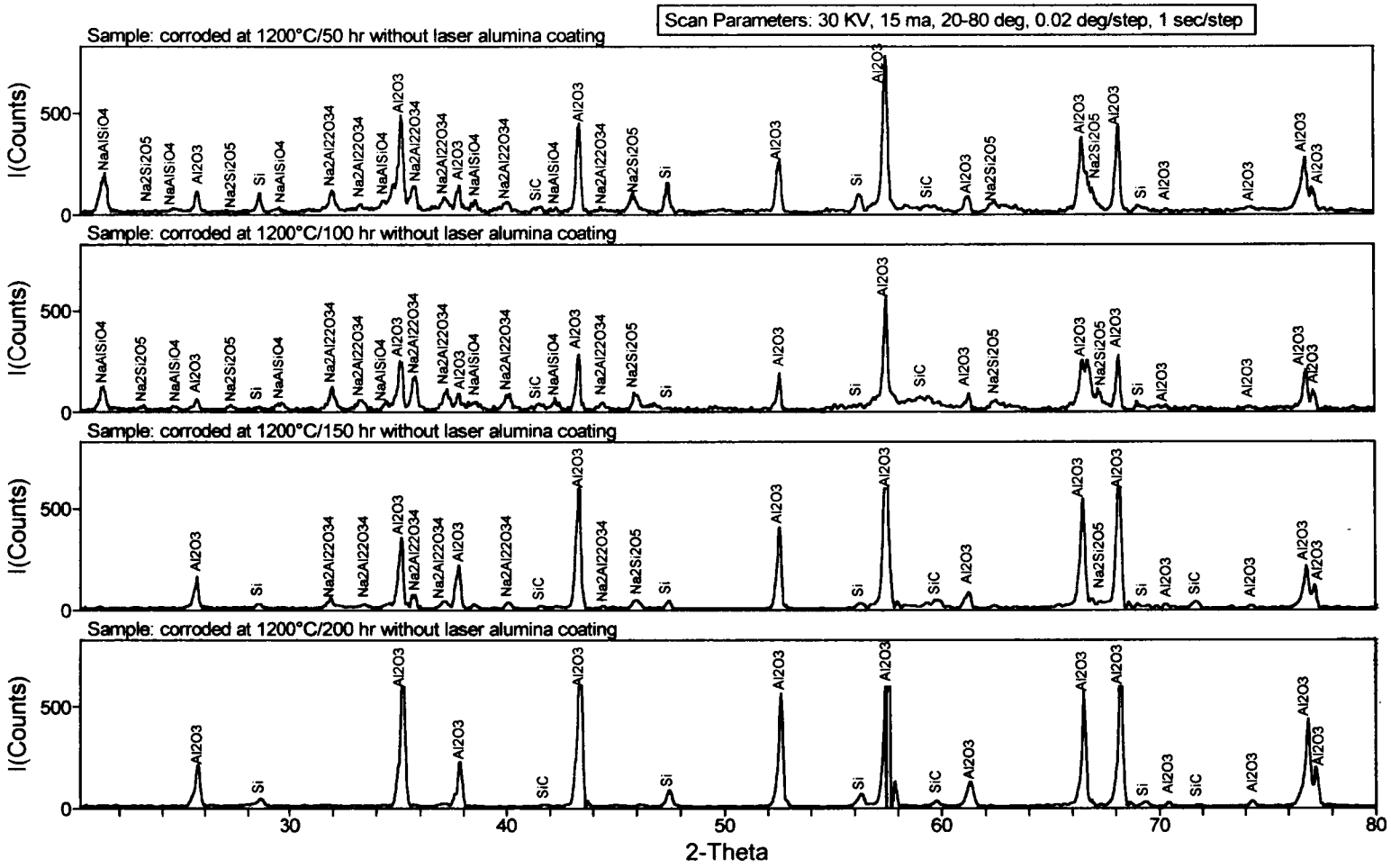

Figure 4-18. X-ray diffraction patterns of specimens without laser-induced reaction alumina coating before corrosion products were removed by a HF solution

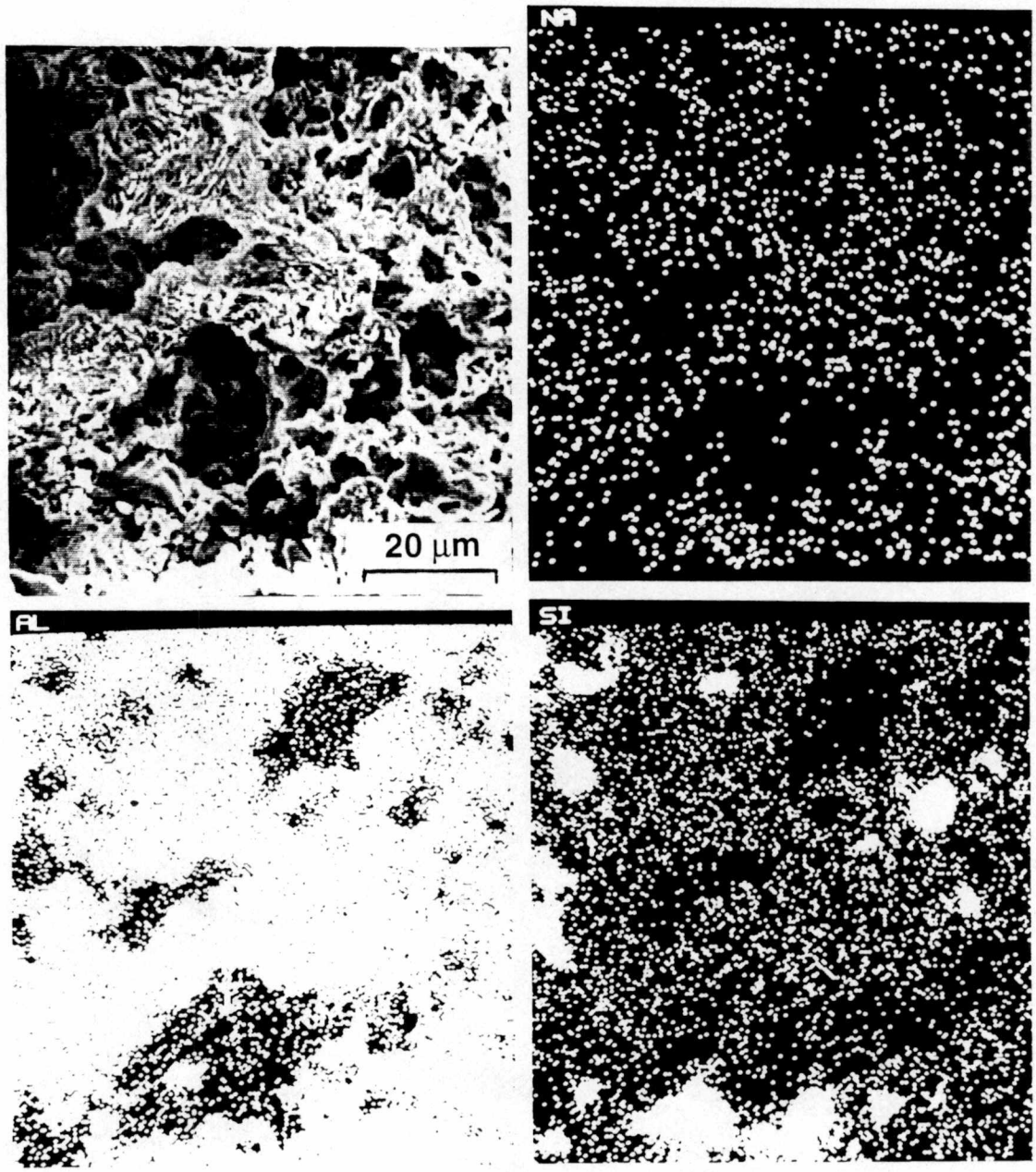

Figure 4-19. SEM photograph of a surface view of structure underlying glass phase (glassy phase removed with a HF solution) and elemental x-ray maps.

specimens (same as uncoated samples). Compared with the uncoated samples, the alumina coated samples experienced a much smaller weight increase. The edge areas of the specimens were not processed during the laser coating processing, thus these areas should experience the same corrosion as the specimens without the laser-induced reaction alumina coating. This edge effect would attribute to some of the weight increase for the laser coated specimens. If the surface of specimens was totally covered by the laser-induced reaction alumina coating, the weight change would be even less.

Figure 4-20 shows optical micro-photographs of cross-sectional views of the specimen coated with the laser-induced reaction alumina coating and the specimen with the laser-induced reaction alumina coating exposed at 1200°C for 200 hours corrosion after washing with a HF solution. Figure 4-21 is SEM photograph of the cross-sectional view and elemental x-ray maps of the SiC_P/Al_2O_3 composite with a laser-induced reaction alumina coating corroded at 1200°C for 50 hours after washing with a HF solution. Both Figures 4-20 and 4-21 show that the laser coated samples experienced very little attack on the outside surface of the coating, no defects appeared in the joint interface between the substrate and the coating after the corrosion test, and none of the composite under the coating was attacked. This indicates that the laser-induced reaction alumina coating provided an effective protection to the composite and that the bonding between the composite and the laser-induced reaction alumina coating was excellent. It also prevented aluminum from extruding to the composite surface as there was no Si/Al_2O_3 oxidation product formed on the surface of the coating. This might be the

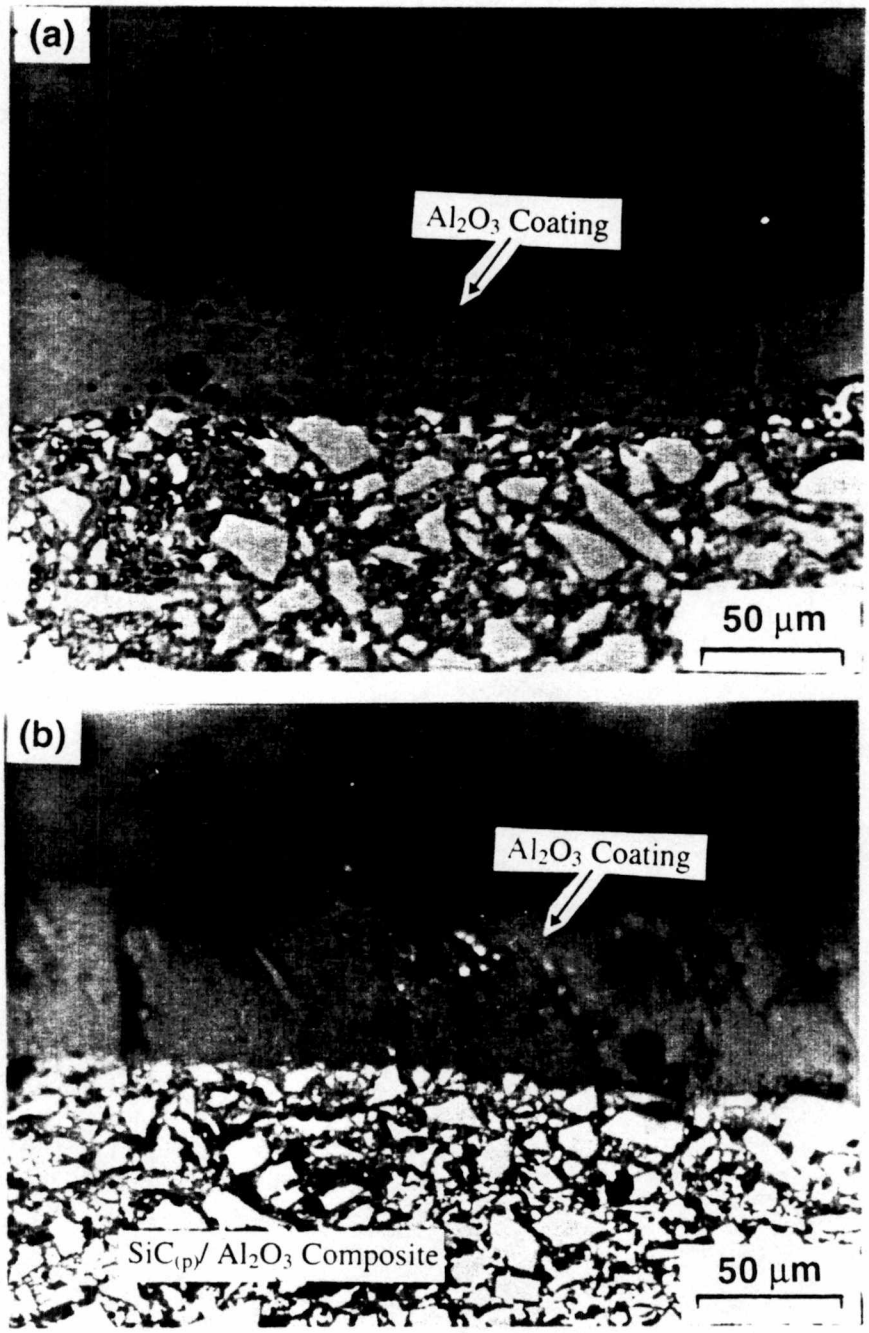

Figure 4-20 Optical microphotographs of cross-sectional views for the specimens: (a) as-coated with the laser-induced reaction alumina coating, (b) the specimen with the laser-induced reaction alumina coating exposed at 1200°C for 200 hours corrosion after washing with a HF solution.

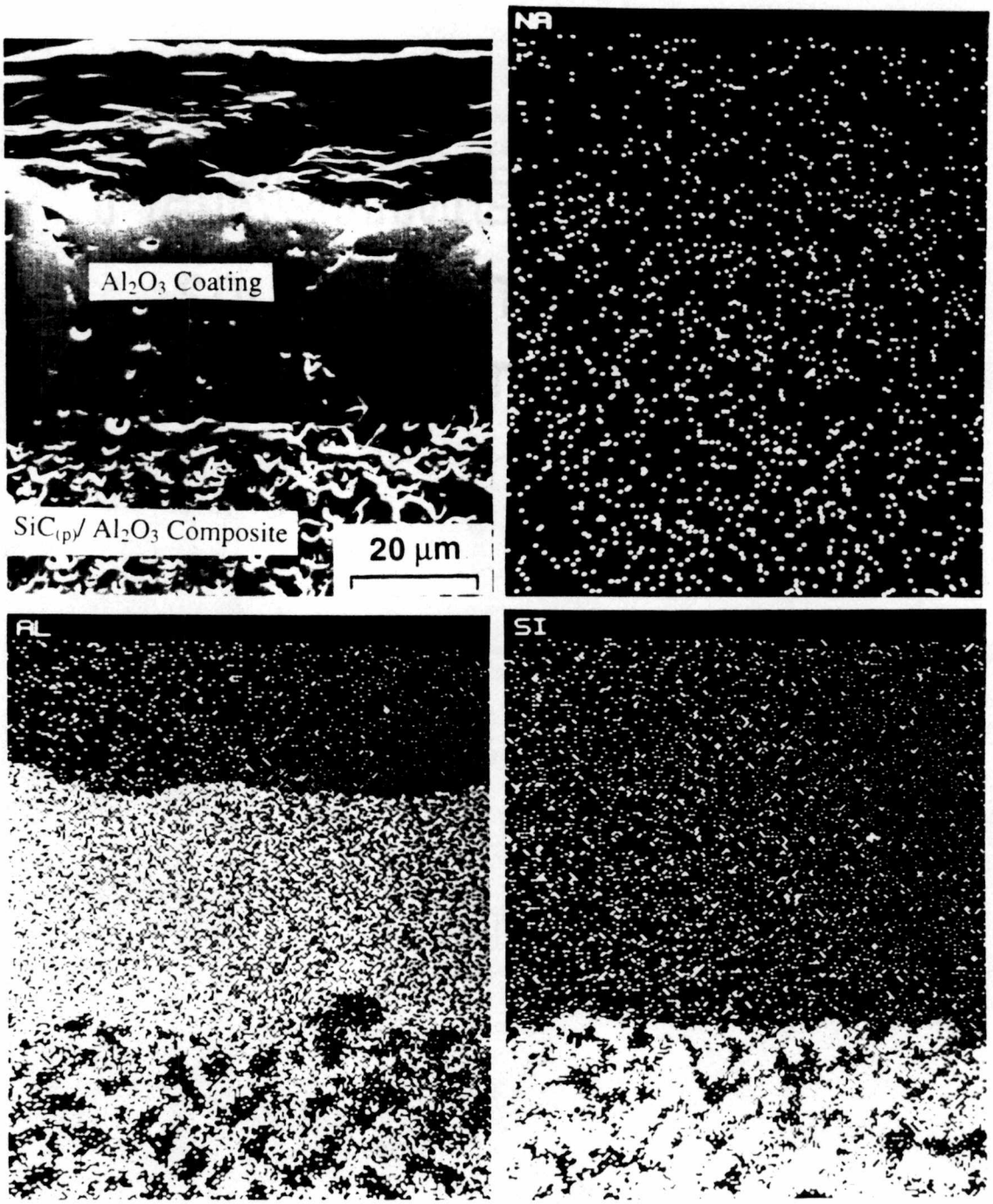

Figure 4-21. SEM photograph of a cross-sectional view and elemental x-ray maps of the SiC_P/Al_2O_3 composite with the laser-induced reaction alumina coating corroded at 1200°C for 50 hours after washing with a HF solution.

reason that the weight change of the coated specimens was much less than the uncoated specimens.

Figure 4-22 pictures x-ray diffraction patterns of specimens with the laser-induced reaction alumina coating before corrosion products were removed by a HF solution. It shows $Na_2OAl_2O_3SiO_2$ and $Na_2Al_{22}O_{34}$ formed on the surface of the composite during corrosion testing. Both $Na_2OAl_2O_3SiO_2$ and $Na_2Al_{22}O_{34}$ are highly refractory due their high melting points. The melting points are approximately 1500°C and 2000°C,[97] respectively. Therefore, the laser-induced reaction alumina coating protects the SiC_P/Al_2O_3 composite from corrosion by at least two means: Firstly, the coating is almost an impenetrable layer to corrodents such as salt and oxygen. Secondly, the coating lessens the effect of the reaction by becoming part of the corrosion product. By introducing one or more refractory compounds into the corrosion product, the refractoriness of the SiO_2-rich layer is increased. For example, all compositions in the Na_2O-SiO_2 binary system are partially or totally liquid at temperatures above approximately 1200°C,[96] whereas certain compositions in the Na_2O-SiO_2-Al_2O_3 ternary system are solids at the same temperature.[97] A coating containing a high Al_2O_3 content might equalize beneficially with the chemically altered SiO_2 layer. Figure 4-23 shows x-ray diffraction patterns of the specimens with the laser-induced reaction alumina coating after the corrosion products were removed by a HF solution. It indicates silicon and silicon carbide was detected by the x-ray diffraction analysis. The trace amount of Si and SiC detected are attributed to the edge effect (no coating) of the alumina coated specimens.

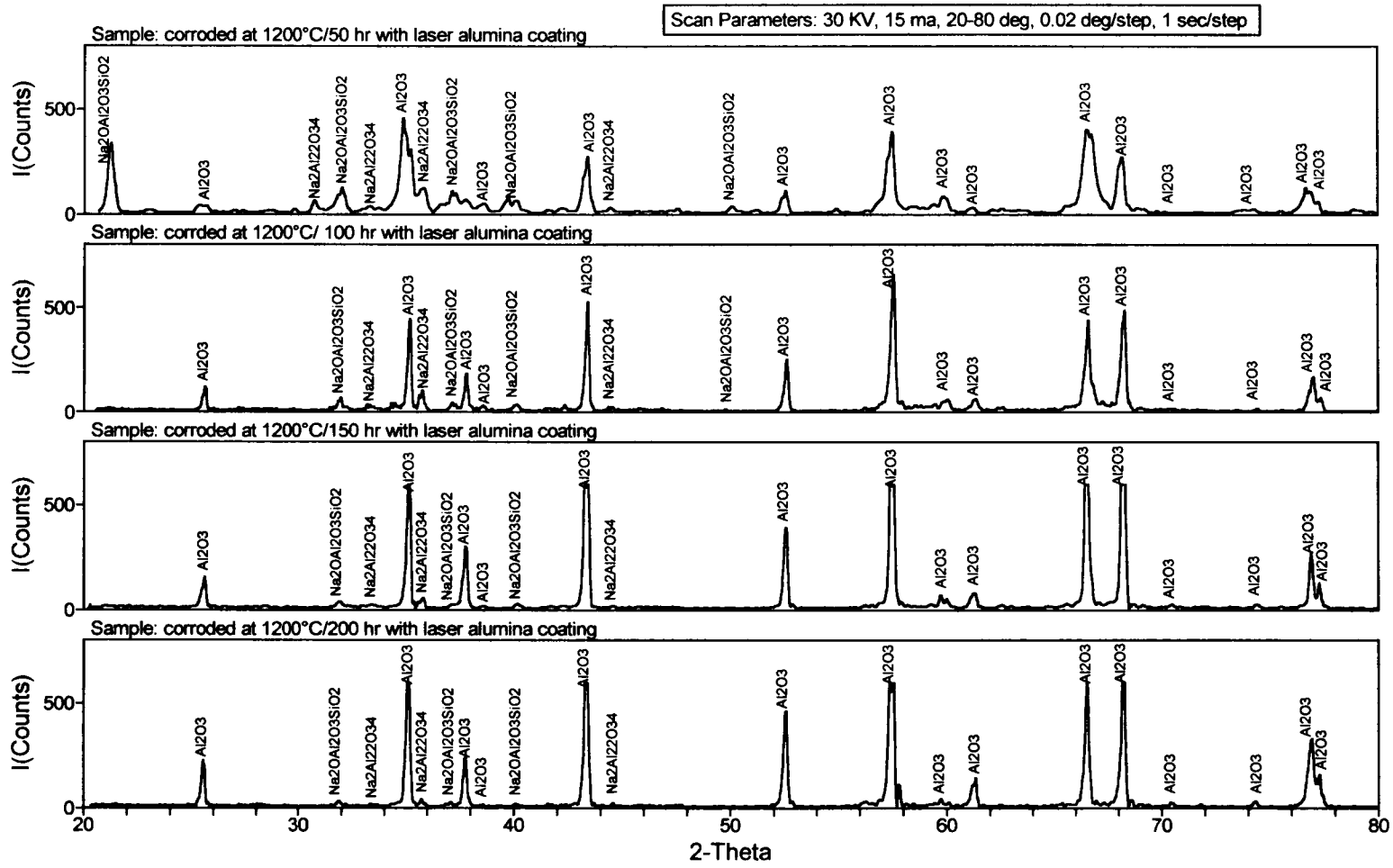

Figure 4-22 X-ray diffraction patterns of specimens with the laser-induced reaction alumina coating before the corrosion products removed by HF solution

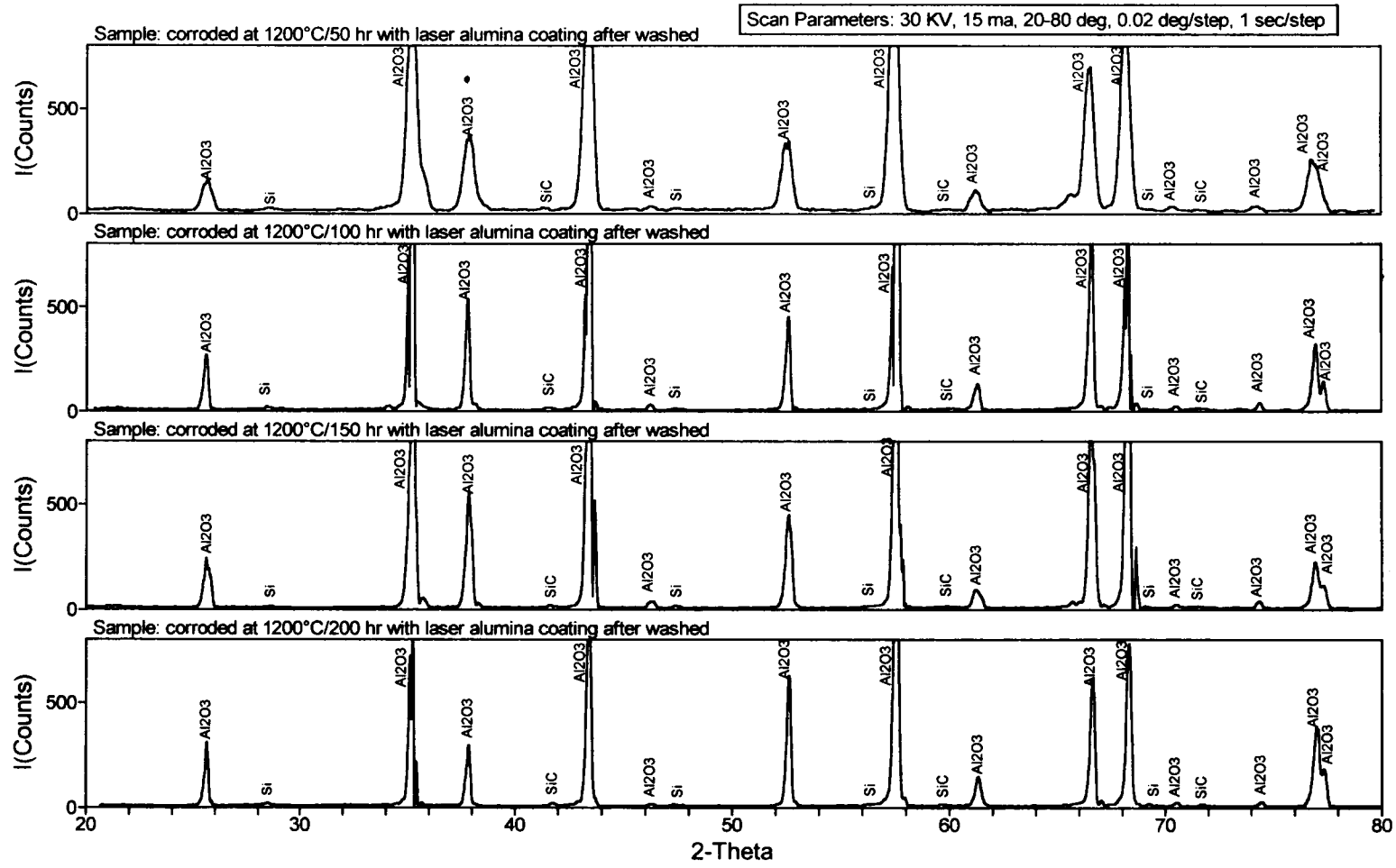

Figure 4-23 X-ray diffraction patterns of specimens with the laser-induced reaction alumina coating after the corrosion products removed by a HF solution

CHAPTER 5

CONCLUSIONS

1. An alumina coating of about 50 micron thickness was successfully deposited on the $SiC_{(P)}/Al_2O_3$ ceramic composite substrate using a laser-induced reaction technique. The coating appeared to be adherent to the substrate and free of cracks and porosity, although a few surface microcracks were observed. X-ray diffraction analysis indicated that the entire coating was alumina.
2. The evaluation of the coated samples in comparison with the as-received samples based on three-point bending test results indicated a strength reduction of about 14%. This may be due to thermal shocking and micro-cracking introduced by the laser coating process.
3. For the uncoated samples:
    A. The SiC_P/Al_2O_3 composite initial experienced an increase in weight during the exposure to Na_2CO_3 at 1200°C due to the oxidation of residual aluminum metal in the composite. There was no significant weight change difference experienced during exposure times between 50 and 200 hours.
    B. The oxidation layer formed on the as-received composite surface consisted of Si and Al_2O_3 (after washing with a HF solution). The oxidation layer grew outward and inward from the original surface of the composite. The growth rate in the outward direction was faster than in the inward direction.

C. The formation of the Si/Al_2O_3 oxidation layer on the as-received composite was nonuniform, and localized corrosion was observed.

4. For coated samples:

   A. The laser-induced reaction alumina coating effectively provided protection for the SiC_P/Al_2O_3 composite by the keeping corrodents from contacting the composite and by the formation of some refractory compounds such as $Na_2OAl_2O_3SiO_2$ and $Na_2Al_{22}O_{34}$.

   B. After exposure to 1200°C for 200 hours, the bonding between the laser-induced reaction alumina coating and the composite appeared to be unattacked.

5. For both the coated and uncoated samples, porosity within the composite increased after exposure due to the reaction: $3SiO_2(s) + 4Al(l) \rightarrow 2Al_2O_3(s) + Si(s)$.

LIST OF REFERENCES

1. R. A. Penty and J W. Bjerklie, "Silicon Carbide for High Temperature Heat Exchangers," *Ceramic Engineering and Science Proceedings*, pp. 120-127 (1982)
2. C. Wagner, "Passivity During the Oxide of Silicon at Elevated Temperatures," *J. Appl. Phys.*, vol. 29, pp. 1295-1297(1958)
3. Z. Zheng, R E. Tressler, and K E. Spear, "Oxide of Single Crystal Silicon Carbide: Part I, Experimental Studies," *J. Electrochem. Soc*, vol. 137, pp. 854-858(1990)
4. J. L. Smialek and N. S. Jacobson, "Mechanism of Strength Degradation for Hot Corrosion of α-SiC," *J. Am. Ceram. Soc.*, vol. 69, no. 10, pp. 741-752 (1986)
5. M. Shimada, T. Sato, Y. Koike and T. Endo, "Corrosion and Degradation in Strength of Silicon Nitride Based Ceramics by Alkali Surface and Carbonate Melts," *Adv. Mats.*, vol. 4, Materials Research Society (1989)
6. N. S. Jacobson, J. L. Smialek and D. S. Fox, "Molten Salt Corrosion of Ceramics," *Corrosion of Advanced Ceramics*, edited by K. G. Nickel. Kluwer, Academic Publishers (1993)
7. A. Gadalla, M. Elmasry, P. Kongkachuichay, "High Temperature Reactions within SiC/Al_2O_3 Composites," *Journal of Materials Research,* vol. 7 No. 9, pp. 2585-2592 (1992)
8. W. Kern, R. E. Tressler and M. J. Mcnallan, "Durability of SiC/Al_2O_3 Composites in Contact with Sodium Silicate," *News letter, Center for Advanced Materials,* Penn. State Univ. (1992)

9. N. S. Jacobson, "Corrosion of silicon Based Ceramics in Combustion Environments," *J. Am. Cerm. Soc.*, vol. 776, pp. 3-28 (1993)

10. M. I. Mayer and F L. Riley, "Sodium Assisted Oxidation of Reaction Bonded Silicon Nitride," *J. Mater. Sci.*, Vol. 13, pp. 1319-1328 (1978)

11. Z. Zheng, R E. Tressler, and K E. Spear, "The Effect of Sodium Contamination on the Oxidation of Single Crystal Silicon Carbide," *Corros. Sci.*, Vol. 33, pp. 545-556 (1992)

12. Z. Zheng, R E. Tressler, and K E. Spear, "A Comparison of the Oxidation of Sodium Implanted CVD Si_3N_4 with Oxidation of Sodium Implanted SiC Crystals," *Corros. Sci.*, Vol. 33, pp. 569-580 (1992)

13. N. S. Jacobson and J L. Smialek, "Hot Corrosion of Sintered Alpha SiC at 1000 °C," *J. Am. Ceram. Soc.*, Vol. 69, pp. 432-439 (1985)

14. N. S. Jacobson, "Kinetics and Mechanism of Corrosion Alpha SiC by Molten Salts," *J. Am. Ceram. Soc.*, vol. 69, pp. 74-82 (1986)

15. N. S. Fox and N S. Jacobson, "Molten Salt Corrosion of Silicon Nitride: I, Sodium Carbonate," *J. Am. Ceram. Soc.*, vol. 71, pp. 128-138 (1988)]

16. J. I. Federer and P. J. Jones, "Oxidation/Corrosion of Metallic and Ceramic Materials in an Aluminum Remelt Furnace," *ORNL/TM-9741, Oak Ridge National Laboratory*, Oak Ridge, Tennessee, (December 1985)

17. J. I. Federer, *1st Int. Ceramics Science & Technology Congress*, paper no. 27-SXV-89C, Anaheim, CA. (1989)

18. N. Birks, G. H. Meier and F. S. Pettit, "Forming Continuous Alumina Scales to Protect Superalloys,". *JOM*, vol. 46, no. 12, pp. 42-46 (1994)

19. W. D. Kingery, H. K. Bowen, and D. R. Uhlmann, *Introduction to Ceramics,* 2nd ed, pp. 240, John Wiley & Sons, Inc, New York (1976)

20. J. L. Smialek and G. H. Meier, "High Temperature Oxidation," *Superalloys II*, ed. C. T. Sims, N. S. Stoloff, W. C. Hagel, pp. 295, New York, NY: John Wiley and Sons (1987)

21. V. Goldfarb, "Materials Testing for an Advanced Glass Melter Heat Exchanger," *GRI Contract No. 5086-232-1274, Final Report*, Gas Research Institute, Chicago, Illinois. (1988)

22. J. I. Federer and P. J. Jones, "Oxidation/Corrosion of Metallic and Ceramic Materials in an Aluminum Remelt Furnace," *ORNL/TM-9741, Oak Ridge National Laboratory*, Oak Ridge, Tennessee, (December 1985)

23. G. C. Wood, *Oxidation of Metals and Alloys*, pp. 201 Metal Park, OH: ASM (1971)

24. C. A. Barrett and C E. Lowell, Oxide. Metas., pp. 199, 11(1977)

25. J. Schienl, and J. Smyth, "High Temperature Coating Study to Reduce Contact Stress Damage of Ceramics," *ORNL/Sub/84-47992/1*, Oak Ridge National aboratory, Oak Ridge, Tennessee, March (1987)

26. Federer, "An Investigation of Ceramic Coating for Protection of SiC from High Temperature Corrosion," *Oak Ridge National Laboratory*, Oak Ridge, Tennessee, (1990)

27. J. P. Pollinger & G. L. Messing, *Mat. Sci. Res.*, vol. 17, pp. 505-510 (1984)

28. A. R. Cooper, "Kinetics of Refractory Corrosion," *Ceram. Eng. Soc. Proc. 2*,

29. W. D. Kingery, H K. Bowen and D R. Uhlmann, *Introduction to Ceramics*, 3rd edition, Wiley, (1989)

30. A. R. Cooper, Jr. and K D. Kingery, "Dissolution in Ceramic Systems: I Molecular diffusion, Natural Convection and forced Convection Studies of Sapphire Dissolution in Calcium Aluminum Silicate," *J. Am. Ceram. Soc.*, vol. 47, no 1, pp. 37-43 (1964)

31. M. Millard, M. Wuttig and H U. Anderson, "Influence of Grain Boundaries on Liquid Corrosion of Al_2O_3 and NaCl," paper no. 76-SII-82, *Am. Ceram. Soc.*, May 1982

32. K. K. Kappmeier, "The Importance of Microstructure Considerations in the Performance of Steel Plant Refractories," in *Ceramic Microstructures*, R M. Fulrath and J A. Pask eds. Wiley, pp. 22 (1968)

33. D. Cubicciotti and K H. Lau, "Kinetics of Oxidation of Hot-Presses Silicon Nitride Containing Magnesia," *J. Am. Ceram.* Soc. vol. 61, pp 512-517 (1978)

34. S. C. Singhal, "Oxidation Kinetics of the Hot Pressed SiC," *J. Mat. Sci.* vol. 11, pp. 246-1253 (1976)

35. R. A. Gardner, "The Kinetics of Silica Reduction in Hydrogen," *J. Solid state Chem.* vol. 9, pp. 336-344 (1974)

36. M. S. Crowley, "Hydrogen-Silica Reactions in Refractories," *Bull. Am. Ceram. Soc.* vol. 46, pp. 679-682 (1967)

37. H.R. Kim, "Gaseous Corrosion of Oxide Ceramics," *M S. Thesis*, University of Pittsburgh (1983)

38. L. J. Trostel, Jr, "Stability of Alumina and Zirconia in hydrogen," *Am. Ceram. Soc. Bull.*, vol. 44, pp 950-952 (1965)

39. J. R. Blachere and F S. Pettit, "high Temperature Corrosion of Ceramics," *DOE/ER/10915-4*, University of Pittsburgh, Pittsburgh, PA (1984)

40. W. L. Fielder, "Oxidation and Hot Corrosion of Hot-pressed Si_3N_4 at 1000 °C," *NASA-TM-86977*, NASA Lewis Research Center, Cleveland, OH (1985)

41. N. S. Jacobson, "Kinetics and Mechanism of Corrosion of SiC by Molten Salts", *J. Am. Ceram. Soc.*, vol. 69, pp. 74-82 (1986)

42. W. C. Bourne and R E. Tressler, "Molten Salt degradation of Si_3N_4 Ceramics," *Am. Ceram. Soc. Bull*, vol. 59, no. 4, pp. 443-452 (1980)

43. G. C. Wei and C L. White, "High Temperature Behavior of Pressureless-Sintered SiC in a Steel Soaking Pit Environment," *Am. Ceram. Soc. Bull*, vol. 63, pp. 890-893 (1984)

44. M. K. Feeber, J. Ogle, V J. Tennary and T. Henson, "Characterization of Corrosion Mechanisms Occurring in a Sintered SiC Exposed to Basic Coal Slags," *J. Am. Ceram. Soc.*, vol. 68, pp. 191-197 (1985)

45. J. W. Adam and D C. Larsen, "Evaluation of Corrosion/Erosion Behavior of Various Ceramic Materials," *AFWALTR-84-4067*, IIT Research Institute, Chicago, IL (1984)

46. D. W. McKee and D. Chatterji, "Corrosion of Silicon Carbide in Gases and Alkaline Melts," *J. Am. Ceram. Soc.*, vol. 59, pp. 441-444 (1976)

47. L. M. Sheppard, "Automotive Performance Accelerates with Ceramics," *Am Ceram. Soc. Bull.*, vol. 69, pp 1012 (1990)

48. M. M. Dosbson, *Silicon Carbide Alloys* (Parthenon Press, Carnfoarth, Lancashire, England) pp. 1-5 (1986)

49. W. J. Lacky, D P. Stinton, G A. Cerny, A C. Schaffauser, and L L. Fehrenbacher, *Adv. Ceram. Mater.* vol. 2, pp. 24 (1987)

50. H. E. Helms, P W. Heitman, L C. Lindgren, and S R. Thrasher, *Ceramic Applications in Turbine Engines* (Noyes Publications, Park Ridge, NJ), pp. 143-237 (1986)

51. D. W. Richerson, *Modern Ceramic Engineering* (Marcel Dekker, In, New York), pp 126 (1982)

52. S. C. Singha, "Corrosion Behavior of Silicon Nitride and Silicon Carbide in Turbine. Atmospheres," *Proceedings of the 1972 Tri-Dervice Conference on Corrosion*, MCIC 73-19, pp. 245-250 (1979)

53. D. W. McKee and D. Chatterji, "Corrosion of Silicon Carbide in Gases and Alkaline Melts," *J. Am. Ceram. Soc.* vol. 59, pp. 441-444 (1976)

54. D. W. Richarerson and T M. Yonushonic, "Environmental Effects on the Strength of Silicon Nitride Materials," in *DARPA/NAVSEA Ceramic Gas Turbine Demonstration Engine Program Review*, MCIC Report MCIC-78-36, pp. 247-271 (1978)

55 K. Natesan, "Corrosion and Mechanical Behavior of Materials for Coal Gassification Applications", *Argonne National Laboratory, Report ANL80-5*, Argonne, Illinois (1980)

56. R. A. Perkins and S J. Vonk, "Materials Problems in Fluidized-Bed Combustion Systems, IV-Corrosion Chemistry in Low-Oxygen Activity Atmospheres," *EPRI Report FP-1280* Electric Power Research Institute (1979)

57. T. E. Easler, "Corrosion Behavior and Mechanical Properties of Silicon Carbide Exposed to a Coal Gasification Environment," *Argonne National Laboratory, Report ANL/FE-84-21*, Argonne, Illinois (1985)

58. G. L. Ridderbusch, "Glass melting furnace: Recent Developments in Process and Materials Technology," *Center for advanced Materials Newsletter*, vol. 4, no. 2, pp. 89-90, 98-103 (1990)

59. V. Goldfarb, "Materials Testing for Advanced Glass Melter Heat Exchanger," *Report No. 88/0155.* Gas Research Institute, Chicago, IL (1988)

60. D. P. Butt and J J. Mecholsky, "Study of the Corrosion of Ceramic Materials in a Simulated Advanced Glass Melter Flue-Gas Environment," *Report No. 88/0134.* Gas Research Institute, Chicago, IL (1988)

61. M. S. Newkirk, H D. Lesher, D R. White, C R. Kennedy, A W. Urquhart, and T D. Claar, "Preparation of Lanxide™ Ceramic Matrix Composites: Matrix Formation by the Directed Oxidation of Molten Metals," *Ceramic Engineering and Science Proceedings*, vol. 8, pp. 879-882 (1987)

62. M. S. Newkirk, A W. Urquhart, H R. Zwicker, and E. Breval, "Formation of Lanxide™ Ceramic Composite Materials," *Journal of Materials Research*, vol. 1, no. 1, pp. 81-89 (1986)

63. M. K Aghajanian, N H. MacMillan, C R. Kennedy, S J. Luszcz, and R. Roy, "Properties and Microstructures of Lanxide™ Al_2O_3-Al Ceramic Composite Materials," *Journal of Materials Science*, vol. 24, no. 2, pp. 658-670 (1989)

64. W. A. Kern, R E. Tressler and M J. McNallan, "Durability of SiC/Al_2O_3 Composites in Contact with Sodium Silicate," *Center for Advanced Materials*, vol. 6, no. 1, pp. 1-6 (1992)

65. W. H. Boss and S. Babu, "An Investigation into the Feasibility of a Radiant Recuperative Air Heater for a Magnetohydrodynamic/Steam Power Plant-Topical Report," *DOE-ET-10815-139*, pp. 110-111, United States Department of Energy (1991)

66. J. P Winkler, "An Evaluation of a Silicon Carbide /Alumina Ceramic Composite for Use in High Temperature Air Heaters," *MS Thesis*, University of Tennessee Space Institute (1992)

67. P. F. LaRue, "An Evaluation of the Strength of a $SiC_{(P)}/Al_3O_3$ Ceramic Matrix Composite Exposed to Coal Slag at Elevated Temperatures," *MS Thesis*, University of Tennessee Space Institute (1995)

68. J. I. Federer, "Corrosion of SiC Ceramics by Na_2SO_4," *Advanced Ceramic Materials,* vol. 3, no. 1, pp. 55-61 (1988)

69. D. S. Gnanamuthu, "Cladding," *US Patent*, 3942180, April 20, 1976

70. J. Powell and W. M. Steen, "Vibro Laser Cladding," *Laser in Metallurgy*, edited by K. Mukherjee and J. Mazumder, Conference Proceedings published by the Metallurgical Society of AIME (1981)

71. J. D. Ayers, R. J. Schaefer, and W. P. Robey, "A Laser Processing Technique for Improving the Wear Resistance of Metals," *Journal of Metals*, August, 1981

72. D. Crucian, G. Molino, M. Musci, E. Borsella and R. Fantoni, "Applications of Laser for Ceramic Alloy on Metallic Surface," *IL NUOVO CIMENTO*, vol. 11D, no. 3, pp. 495-502 (1989)

73. E. Vandehaar, P. A. Molian, and M. Baldwin, "Laser Cladding of Thermal Barrier Coatings," *Surface Engineering*, vol. 4, no. 2, pp. 159-172 (1990)

74. E. Ramous, L. Giordano, A. Tiziani, B. Badan and M. Cantello, "Laser Cladding of Ceramic and Metallurgic Coatings on Steel," *Key Engineering Materials*, vol. 46, pp. 425-434 (1990)

75. K. M. Jasim, R. D. Rawlings, D. R. F. West, "Thermal Barrier Coatings Produced by Laser Cladding," *J. of Materials Science*, vol. 25, pp. 4943-4948 (1990)

76. W. M. Steen, R. M. Vilar, K. G. Watkins, M. G. S. Fereira "Alloy System Analysis by Laser Cladding," *Proceedings of the Laser Materials Processing Symposium*, pp. 278-287, ICALEO'1992

77. G. C. Irons, "Laser Fusing of Flame Spray Coatings," *Welding Journal Research Supplement*, (December 1978)

78. J. D. Ayers and R. J. Schaefer, "Consolidation of Plasma Sprayed Coating by Laser Remelting," *SPIE Vol. 198 Laser Applications in Materials Processing*, (1979)

79. Nobuya Iwamato and Norimasa Umesaki, "Surface Treatment of Plasma-sprayed Ceramic Coatings by a Laser Beam," *Surface and Coatings Technology*, vol. 34, pp 59-67 (1988)

80. L. Mannik, A. V. Manolescu, J. O. Noga, S. K. Brown and A. G. McMillan, "Laser Modified Coatings for Energy Systems," *Proceedings of the Laser Materials Processing Symposium*, pp. 237-250, ICALEO'1992

81. R. Veltri and F. Galasso, "Effect of Continuous-Wave High Intensity Laser Radiation on the Strength of Silicon Nitride and Silicon Carbide," *J. Am. Ceram. Soc*, vol. 65, no. 4, pp. 49-53 (1982)

82. F. Galasso and R. Veltri, "Observations of Laser Interactions with Ceramics," *Am. Ceram. Soc. Bull*, vol. 62, no. 2, pp. 253-254 (1983)

83. T. R. Anthony and H. E. Cline, "Surface Rippling Induced by Surface Tension Gradients during Laser Surface Melting," *J. Appl. Phys.*, vol. 48, pp. 3888-3894 (1977)

84. I. C. Hawkes, M. Lamb, W. M. Steen and D. R. F. West, "Surface Topography and Fluid Flow in Laser Surface Melting," *Proc. 3rd CISFEL Conf.,* Lyon, France. pp.125-131 (Sept., 1983),

85. N. B. Dahotre, C. Xiao, B. Boss, M. H. McCay and T. D. McCay, "Evolution of Microstructure and Mechanical Properties in Laser Induced Reaction Coating of Al_2O_3 on SiC/ Al_2O_3 Composite", *in Elevated Coatings: Science and Technology II*, Eds. N. B. Dahotre and J. M. Hampikian, Proceeding of a Symposium, TMS Annual Meeting 96 in Anaheim, California, pp.441-452, February 1996

86. D. R. Gaskell, "*Introduction to Metallurgical Thermodynamics*," second edition. Hemisphere Publishing Corporation, pp.585 (1981)

87. W. D. Kingery, H. K. Bowen and D. R. Uhlmann, "*Introduction to Ceramics*," 2nd ed. pp. 240 (New York: John Wiley & Sons, 1976)

88. N. B. Dahotre, C. Xiao, B. Boss, M. H. McCay and T. D. McCay, "Coating Ceramic Composites by a Laser In-Situ Reaction Technique," *JOM* (J. of Minerals, Metals and Materials Society), vol. 47, no. 10, pp.51-53, 1995

89. N. B. Dahotre, C. Xiao, B. Boss, M. H. McCay and T. D. McCay, "Laser Induced Surface Modification of Ceramic Coated Ceramic Composite for High Temperature Corrosion Protection," in Elevated Temperature Coatings: Science and Technology-I, Eds. N. B. Dahotre, J. M. Hampikian and J. J. Stiglich, the Metallurgical Society of AIME, Warrendable, PA, pp. 113-123, 1995

90. N. B. Dahotre, C. Xiao, B. Boss, M. H. McCay and T. D. McCay, "Laser Induced Reaction Coatings of Ceramics," in Surface Modification Technologies VIII, Eds. S. Sudarshan and M. Jeandin, the Institute of Materials, London, UK, pp. 310-319, 1995.

91. M. W. Chase , Jr., C. A. Davies, J. R. Downey, Jr., D. J. Frurip, R. A. McDonald, and A. N. Syverud, "JANAF Thermochemical Tables" 3rd ed., *The American Chemical Society and the American Institute of Physics*, New York (1986)

92. DuPont Lanxide Composites Inc., *Product Catalogue*.(February, 1995)

93. Kristin Breder and Randy J. Parten, "Strength and Corrosion Behavaior of SiC-Based Ceramics in Coal Combustion Environments," *Proceedings of the Tenth*

Annual Conference on Fossil Energy Materials, pp.55-62, Knoxville, Tennessee.(May, 1996)

94. W. A. Kern, M. J. McNallan and R. E. Tressler, "Oxidation and Corrosion of $SiC_{(paticulate)}/Al_2O_3$ Composites in Sodium Silicate at Elevated Temperatures," *J. Am. Ceram. Soc.*, vol. 79 (7), pp. 1881-91 (1996)

95. ASM Handbook Committee, *Metals Handbook*, 8th edition, vol. 8, pp. 263, Metals Park, Ohio (1973)

96. Margie K. Reser, *Phase Diagram for Ceramists*, vol. 1, pp. 84, the American Ceramic Society, fifth printing, 1985

97. Margie K. Reser, *Phase Diagram for Ceramists*, vol. 1, pp. 181, the American Ceramic Society, fifth printing, 1985

VITA

Chenghe Xiao was born in Chengdu, Sichuan, China on October 22, 1956. He received his middle and high school education from the 24th school of Chengdu, China from September of 1969 to July of September of 1974. He attended Zhejiang University in Hangzhou, China from which he received his Bachelor of Science degree in Materials Science and Engineering in July of 1982. After graduation, he spent two years working in a steel mill as a Assistant Metallurgical Engineer. He began his graduate studies again at Zhejiang University in September of 1984. He received his Master of Science degree in Materials Science and Engineering in June of 1987, after which he worked as a Research Engineer and Instructor in Zhejiang University for five years. He jointed the University of Tennessee Space Institute in January of 1993 and received his Doctor of Philosophy degree in Engineering Science and Mechanics in May of 1997.